

National Aeronautics and Space Administration
Research Grant NGR 39-087-003

THE EFFECT OF MICROSTRUCTURE AND
STRENGTH ON THE FRACTURE TOUGHNESS
OF AN 18 Ni, 300 GRADE
MARAGING STEEL

by

J. A. Psioda and J. R. Low, Jr.

(NASA-CR-143501) THE EFFECT OF
MICROSTRUCTURE AND STRENGTH ON THE FRACTURE
TOUGHNESS OF AN 18 Ni, 300 GRADE MARAGING
STEEL (Carnegie-Mellon Univ.) 92 p HC \$4.75
CSCI 118 63/26

N75-31248

Unclas
35069

Department of Metallurgy and Materials Science
Carnegie-Mellon University
Pittsburgh, Pennsylvania 15213

Technical Report No. 7

August 1975



Distribution of this document is unlimited

This investigation was made possible by a Research Grant
from the National Aeronautics and Space Administration

--	--	--	--	--	--	--	--

This is the annual report on National Aeronautics and Space Administration Grant 39-087-003 for the period from August 1, 1974 to July 31, 1975. The Principal Investigator was Professor John R. Low, Jr. and the NASA Technical Officer was Mr. William D. Klopp, Head, Materials Development Section at NASA Lewis Research Center.

ABSTRACT

The influence of microstructure and strength on the fracture toughness and fracture mechanism of an 18 weight percent Ni, 300 grade maraging steel was examined. This report describes the progress made in this investigation. The 300 grade maraging steel was chosen as a vehicle by which to understand why there exists an inverse relationship between strength and toughness in high strength alloys such as the 18 Ni maraging steels. The 18 Ni, 300 grade maraging material being studied is from a commercial grade consumable-electrode, vacuum arc remelted heat obtained in the form of forged and annealed plate. The matrix contains a population of second-phase impurity inclusions which is a product of the casting and hot working processes. These inclusions do not change with subsequent precipitation hardening. Changes in microstructure resulting in strength increases were brought about by variations in aging temperature and time. Aging conditions included three-hour treatments at temperatures of 316°C (600°F), 329°C (625°F), 344°C (650°F), 371°C (700°F), 399°C (750°F), 427°C (800°F), 482°C (900°F), and 538°C (1000°F). Maximum strength was attained in the 300 grade maraging steel by aging at 427°C (800°F) for 100 hours. Tensile, fatigue precracked Charpy impact, and plane-strain fracture toughness tests have been performed at room temperature, 20°C (68°F). The fracture mode is always dimpled rupture with the morphology changing from large equiaxed dimples in the lowest strength level considered to small dimples, all shallow and irregular. With increasing strength, the fracture toughness decreases as smaller and smaller inclusions can act as sites for void initiation. The fracture behavior of the fully aged and overaged conditions with the

presence of submicron sized dimples suggests the possibility for void coalescence at the strengthening precipitates in the high strength conditions. The microstructure and fracture mechanism of the 300 grade maraging steel as a function of strength level is being studied using optical metallography, electron fractography, thin-foil transmission electron microscopy, and microprobe analyses. Suggestions are made on how the microstructure affects the fracture mechanism and fracture toughness of this high-strength alloy as a function of strength. The types of experiments which are going to be carried out during the remainder of this investigation are also described.

INTRODUCTION

Although considerable emphasis in the past decade or so has been placed on the development of structural metals having high strength-to-density ratios, very little research has been performed to directly link the microstructure to the observed decrease in toughness with increase in strength. Current and developing aerospace and pressure vessel technologies have imposed rather stringent requirements on structures and have necessitated the utilization of materials having a balance of fracture toughness and strength properties. In the attempt to maximize strength and satisfy the unusually high toughness requirements of today's designs, it is apparent that as strength is pushed upward, toughness of a particular high-strength alloy usually drops off quite rapidly. The usual means by which to arrive at the strength-toughness combination compatible with the program goals has been by either drawing from available alloys at various purity levels or by developing an entirely new alloy. The observed inverse relationship between strength and toughness thus necessitates a trade-off between these key material properties.

This report describes the work completed to date on an investigation of the effect of microstructure and strength on the fracture toughness and fracture mechanism of an 18 Ni maraging steel. The alloy chosen for this study is an 18 Ni, 300 grade maraging steel since it can be aged to an extensive range of strengths with an accompanying trend in toughness. An investigation of this commercially significant material may also help in the understanding of the strength-toughness behavior of other high-strength alloys. With an understanding of the interrelationship of strength and toughness, suggestions might be made on how to modify the com-

position and microstructure of the 18 Ni, 300 grade maraging steel so as to improve the fracture toughness without a significant trade-off in strength.

This report gives a brief review of the literature on strength and fracture in 18 Ni, maraging steels and describes the progress of the present investigation. Results which have been reported previously¹ will be summarized in the appropriate sections of the report.

LITERATURE REVIEW

The literature on phase transformations and strengthening mechanisms in 18 Ni maraging steels has been reported in detail previously¹ and only highlights will be given. Deformation and fracture occurs in most 18 Ni maraging steels by the dimpled rupture process.^{2,3,4} The limited work to date that has been devoted to understanding the role of microstructure on the void initiation, growth, and coalescence stages of dimpled rupture will be reviewed.

The 18 Ni, 300 grade maraging steel is based on the binary iron-nickel system. Upon cooling an 18 Ni alloy from the austenite phase field, the austenite transforms to a lath martensite that has a body-centered cubic crystal structure.⁵ The massive martensitic structure of 18 Ni maraging steels consists of a series of elongated laths or platelets that contain a high density of dislocations. There is some evidence that after aging, a massive martensite matrix gives better toughness than a twinned martensite in maraging steels.⁶

Titanium is used in the 18 Ni maraging steels as a supplemental hardener, but the primary strengthening effect comes from the combination of cobalt and molybdenum. Selected-area electron diffraction patterns from an 18 Ni, 300 grade maraging steel indicate that there are two different precipitates within the martensite laths.⁷ With some uncertainty, these precipitates were identified tentatively as an orthorhombic Ni_3Mo phase and a tetragonal $\sigma\text{-FeTi}$ phase.

In addition to the strengthening precipitates, maraging steels contain other particles. The most common second-phase impurity inclusions found

in 18 Ni maraging steels are blocky angular titanium carbonitride particles.^{8,9} Elongated inclusions of titanium sulfides and globular particles of a complex titanium molybdenum phase (probably carbide) have been observed.⁹ Tipper¹⁰ was probably the first to suggest that plastic fracture in single-phase metals originates at voids formed by the drawing away of the matrix from non-metallic inclusions. Many other investigations in several alloy systems have since shown evidence for the role of inclusions in the dimpled rupture of high-strength alloys.^{11,12,13,14} A fractographic study by Birkle and co-workers¹⁵ using several different grades of maraging steel has shown that voids are nucleated at non-metallic inclusions, including various nitrides, carbides, and sulfides, depending upon the exact alloy. In the overaged condition the maraging steels may exhibit void initiation at the strengthening precipitates, as recently shown by Roesch and Henry.² Roesch and Henry² and particularly Cox and Low⁴ show the importance of second-phase impurity inclusions on toughness through fractographic work. They recognize that fracture progresses in stages of void nucleation at inclusions, void growth, and void coalescence.

An extensive fractographic examination of any high-strength alloy, including maraging steel at various strength levels, to determine the relative importance of microstructure on the various stages of fracture as a function of strength level is not in evidence. The decrease in toughness with increasing matrix strength has been observed in several high-strength steels by Fisher and Repko,¹⁶ Jones and Brown,¹⁷ and Srawley.¹⁸ Their work was aimed at developing the size criterion for valid plane-strain K_{IC} testing. The toughness data on maraging steels tested at various strength levels does, however, indicate a strong relationship between strength and toughness. The inverse trend between the strength and toughness properties

is evident in other fracture toughness data from other high-strength alloys including aluminum and titanium.¹⁹

The role of matrix strength level on void initiation is as yet unclear. Roesch and Henry² interpreted their results by assuming that, in order to initiate cavities, the particles must be larger than a certain critical size. The conclusion inferred is that the local concentrated stress at an inclusion of fixed size would be higher in the higher strength condition for the same amount of strain. Gangulee and Gurland²⁰ have studied elongated silicon particles in aluminum-silicon alloys and found that voids form predominately by cracking at lower strains than smaller ones. Cox and Low⁴ have also found that larger particles fail at lower strains than smaller ones in 4340 and 18 Ni, 200 grade maraging steels. Analytical expressions for the elastic stress concentrations within inclusions of specific shapes have been determined by Goodier²¹ and Edwards.²² According to Gurland and Plateau,²³ the initiation of voids is generally preceded by plastic flow of the matrix in the regions of high stress concentration at the inclusions. Gurland and Plateau²³ and also Broek²⁴ have attributed cavity formation to impingement of dislocation pile-ups at inclusions in the manner proposed by Zener²⁵ and analyzed by Stroh.²⁶ Ashby²⁷ had discussed an interesting alternative in which primary deformation incompatibilities do not produce cavities directly, but initiate highly organized secondary slip by punching out dislocation loops from the inclusion-matrix interface to reduce the local shear stresses. The Ashby model of plastic deformation around inclusions can account for void formation by particle-matrix decohesion. McClintock²⁸ has suggested that cavity formation at interfaces may obey a critical local strain criterion, or alternatively a criterion that may be a mixture of a critical interfacial shearing strain

and an interfacial normal stress. Argon and co-workers²⁹ have considered interacting inclusions in a model for cavity formation by interface separation. They²⁹ propose that when the secondary plastic zones of particles touch at large volume fractions of second phase, or at large plastic strains, the interfacial stress becomes dependent also on the local volume fraction of second phase. Argon and Im³⁰ subsequently presented limited experimental evidence that inclusion interactions can enhance the interfacial stress at an inclusion and thus hasten separation. They³⁰ do submit, however, that in order to make further quantitative progress, more accurate solutions for interacting inclusions is necessary.

Titanium carbonitride inclusions in 18 Ni maraging steels have, however, been shown to form voids by particle cracking.⁴ The particle interaction process which Argon and Im³⁰ have described is not the only possibility suggested for explaining the void formation starting preferentially from large inclusions. Gurland³¹ and Cox and Low⁴ have proposed that brittle and cleavable inclusions may have a size dependent strength based on a statistical distribution of flaws. Investigators have shown in steels,⁴ aluminum alloys,³² and a titanium alloy³³ that larger particles nucleate voids at lower stresses. Gurland³¹ has recently observed the size effect for cementite particle cracking in a spheroidized steel. Several possible phenomena to explain the preferential cracking of the largest particles were discussed. An entirely acceptable quantitative explanation for the size effect for void initiation or understanding of the observed microstructural effects is as yet unavailable.

Passoja and Hill³⁴ have developed a theory which can be used to calculate the relationship between fracture toughness and yield stress utilizing the concept of a particle size distribution function for dispersed

second-phase particles in steel. A model³⁵ for the energy absorbed in the ductile fracture of high-strength steels has been presented which incorporates a dissipative energy term and a dislocation storage term. The variable of interest in their³⁵ model is the process zone size which is a characteristic of the material. The process zone size is represented as the mean inter-inclusion spacing on the fracture surface or as the mean linear intercept dimple size on the fracture surface. Passoja and Hill³⁴ stress that a strength-toughness relationship for steel is dependent on the nature of the distribution of second-phase particle sizes present. They also recognize that different types of second-phase particles can be active in the fracture process at different strength levels. These findings appear to apply well to the relative importance of inclusions and strengthening precipitates as a function of matrix strength level in 18 Ni, 300 grade maraging steel.

Metallographic investigations including the work of Floreen and Hayden³⁶ have studied void growth but, until Cox and Low,⁴ no fractographic observations of void growth in maraging steels was carried out. Cox and Low⁴ limited themselves to an 18 Ni, 200 grade maraging steel at a single strength level and single test temperature. Void growth as a function of matrix strength in a single material has not been studied in any work reported in the literature to date. The analysis of Rice and Tracey³⁷ for the stress states existing at inclusions and at the tips of cracks indicates that the rate of void growth increases with increasing strain for both strain-hardening and non-strain-hardening materials. They also indicate that hydrostatic tension should accelerate the rate of void growth. Experimental verification is limited to the fractographic cross-sectioned tensile observations of Cox and Low⁴ and no evidence for the role of strength level

is available.

Void coalescence has been shown to occur by impingement in 18 Ni, 200 grade maraging steel and by void sheet formation at cementite particles in AISI 4340 steel.⁴ Intense shear bands resulting in large slip offsets in the ligaments between neighboring inclusion nucleated voids have been observed by Clausing¹² and Hahn and Rosenfield³⁸ in plane-strain-tension specimens. It is thought that the strain localization in the ligaments may be great enough to cause failure at the strengthening precipitates in aluminum alloys as well as maraging and other high-strength steels.^{2,4,38} As indicated above, the critical size criterion for void initiation may be important for void formation at strengthening precipitates during void coalescence as observed by Roesch and Henry.² Again the behavior of maraging steels and, particularly, the role of strengthening precipitates as a function of matrix strength with respect to the coalescence of inclusion nucleated voids, is unclear.

SCOPE OF THIS INVESTIGATION

The purpose of this investigation is to systematically vary the strength of an 18 weight percent Ni, 300 grade maraging steel by possible variation of both aging time and temperature, isolate any attending microstructural changes, and study the effects of these changes on the fracture toughness and fracture mechanism of this alloy. A 2.0-inch thick plate material of commercial 300 grade maraging steel received a solution anneal at 815°C (1500°F) followed by air cooling. Various aged fatigue precracked Charpy impact specimens were tested at room temperature to establish the magnitude of inverse strength-toughness trend for this material. These data clearly indicated an inverse relationship between strength and toughness more extensive than could potentially be tested for valid plane-strain fracture toughness, K_{IC} , due to the plate thickness limitation of 2.0-inches. The tensile properties, flow curves, and fatigue precracked Charpy impact properties were determined for material aged for 3 hours at 316°C (600°F), 329°C (625°F), 344°C (650°F), 371°C (700°F), 399°C (750°F), 427°C (800°F), 482°C (900°F), 538°C (1000°F); and aged for 100 hours at 427°C (800°F). Valid plane-strain K_{IC} has been determined for the material aged for 3 hours at 427°C (800°F), 482°C (900°F), 538°C (1000°F); and aged for 100 hours at 427°C (800°F).

The fracture modes have been determined for most of these strength levels using transmission electron microscope (TEM) replicas taken from the fracture surfaces of both tensile and K_{IC} specimens. Fracture occurs by the dimpled rupture process at all strength levels considered in the tensile, K_{IC} , and fatigue precracked Charpy impact specimens. Since the dimples in the tensile specimen and fracture toughness specimen fractures

appear to be of about the same size, fracture evidently occurs by a similar mechanism in these two types of tests. Thus, the fracture mechanisms will be studied in smooth round tensile specimens to yield information which should apply to fracture in material subject to plane-strain constraint.

Fractographic examination of additional, lower strength, K_{IC} fractures will be performed as they become available subject to the limitation of the plate thickness. The fracture mechanism as a function of the strength of the 18 Ni, 300 grade maraging steel at 20°C (68°F) will be investigated through the use of quantitative fractography and metallographic sectioning. Quantitative metallography of unstrained material will be used to correlate the microstructure to the fracture mechanism at each strength level. As a function of strength, tensile specimens will be strained to several levels short of fracture. These specimens will be sectioned to study the fracture mechanism as it develops in thick sections. The role that microstructure plays in the void initiation, void growth, and void coalescence stages of dimpled rupture as a function of material strength will be determined. This approach to fracture has made it possible to isolate the differences in fracture mechanism in 4340 and 18 Ni, 200 grade maraging steels⁴ as well as the fracture process in aluminum alloys.³²

This report describes the progress of this research to date.

MATERIALS AND MICROSTRUCTURE

A. Chemical Composition and Processing History

The program heat of 18 Ni, 300 grade maraging steel was of commercial purity made in a regular mill production heat. The material was produced using vacuum induction melting, cast into a 21-inch round electrode, and then vacuum arc remelted into a 25-inch diameter ingot. Subsequent hot working of the ingot was accomplished in two steps, the first of which involved press forging the ingot to a plate 15 inches wide by 3.5 inches thick using a starting temperature of 1150°C (2100°F). After surface conditioning, the plate material was heated to 1150°C (2100°F) and hammer forged to a bar 10.5 inches wide by 2.3 inches thick. Care was taken to avoid exposure of the material for prolonged times at the embrittlement temperature of about 927°C (1700°F).³⁹ The bar was then annealed at 815°C (1500°F), air cooled, and surface ground to the as-received dimensions of 10 inches wide by 2 inches thick. In the annealed condition specimens can be cut from the plate and then aged hardened to selective strength levels.

The chemical specifications for 18 Ni, 300 grade maraging steel, the heat, and check analyses for the program alloy are given in Table I. The compositions are within the specifications. The check and heat analyses of the program alloy are in reasonable agreement based upon the expected error in the check analysis. It is important to note the major elements that are intentional additions and those that are present as impurities. Specifically, Ni, Mo, Co, and Ti alloy additions are all approximately in the middle of their desired ranges. The principal impurity elements, C, S, and P are well below the maximum allowable contents. Particularly, the C and S contents are at one-tenth and one-half their maximum allowable contents,

TABLE I

CHEMICAL ANALYSES OF 300 GRADE,
18 Ni-Co-Mo-Ti MARAGING STEELS
(Weight Percent)

	Commercial Specification	Program Heat Mill Analysis	Program Check Analysis*
C	0.03 Max	0.003	0.002 ± 0.002
Mn	0.10 Max	0.02	0.04 ± 0.01
Si	0.10 Max	0.01	0.03 ± 0.01
S	0.010 Max	0.006	0.005 ± 0.001
P	0.010 Max	0.001	0.005 ± 0.001
Ni	18.0/19.0	18.29	18.53 ± 0.01
Mo	4.6/5.2	4.93	4.77 ± 0.05
Co	8.5/9.5	8.98	8.63 ± 0.1
Al	0.05/0.15	0.10	0.12 ± 0.002
Ti	0.5/0.8	0.63	0.65 ± 0.01
Zr	0.02 Added	0.016	0.015 ± 0.001
B	0.003 Added	<0.001	<0.001 ± 0.001
Ca	0.05 Added	-	0.025 ± 0.01
N ₂	-	-	0.005 ± 0.001
Fe	Balance	Balance	Balance

*Average from two separate test blocks

respectively.

In this heat of 300 grade maraging steel as in any engineering material there is a distribution of second-phase particle sizes and separations. These distributions contain those particles which are added intentionally to alter the material characteristics (strengthening precipitates) as well as other particles which are included incidentally as a result of process limitations. It is important to the overall understanding of microstructural control that we consider the potential forms that C, S, Mo, Ti, and Co can take on. The intentional additions, Ni, Ti, Mo, and Co will preferentially interact in solid-state precipitation reactions during aging treatments to form strengthening precipitates. While precipitates interacting with dislocations in the matrix provide the desired strength, impurity inclusions are detrimental to toughness and hence are undesirable.⁹ Titanium has a high affinity for both carbon and sulfur and hence will tend to combine in the melt with these elements to form inclusions. Since it is difficult, or even impossible, to alter the impurity inclusion distribution below the melting point of the steel, the inclusion population will be fixed throughout this study. Of course, aging will alter the strengthening precipitate distribution and cause a strength change which may or may not influence the fracture toughness. As a function of the degree of aging, it is important to understand the types, sizes, and amounts of second-phase particles present, both precipitates and inclusions, since fracture toughness is largely controlled by the number of active microvoid nucleation sites. Although maraging steels are made to very low C and S concentrations, such melting practice may not be sufficient in itself to guarantee high fracture toughness. In the 200-300 ksi (1378-2068 MN/m²) strength range there is some evidence to indicate that strengthening pre-

cipitates can begin to become active in the fracture process.^{1,2}

B. Aging Conditions

A study aimed at determining the age hardening behavior of the 18 Ni, 300 grade maraging steel was carried out. By variation of both aging time and temperature, mechanical test specimens were aged to attain specified strength levels. For this reason it is important to know the extent of hardening and the kinetics of the age-hardening process as a function of both time and temperature. To this end, an isothermal aging study has been completed. Hardness blanks of 0.25-inch thickness were isothermally aged at 316°C (600°F), 344°C (650°F), 371°C (700°F), 427°C (800°F), 482°C (900°F), and 538°C (1000°F) for times up to 300 hours. Aging treatments were performed in air to parallel the heat treatment procedure necessary for aging toughness specimens which will be as large as 17 inches long by 4 inches wide in the 2-inch thick case. A plot of Rockwell "C" hardness was generated as a function of the logarithm of time at each of these aging temperatures. Each datum point is the average of five hardness indentations per test block. A separate test block was used for each point on the plot presented in Figure 1. As with most age hardenable alloys, the 300 grade maraging steel rapidly overages at a high temperature such as 538°C (1000°F). Although kinetically less rapid, aging at lower temperatures yields a maximum hardness which is greater than that attained at higher temperatures. In this system, loss of hardness (strength) due to overaging is due in part to classical precipitate coarsening and to a time-dependent reversion of the metastable body-centered cubic martensite to the equilibrium face-centered cubic austenite.⁶

Ultimately, isochronal aging treatments will be used to attain various strengths in the relatively thick section toughness specimens. The choice

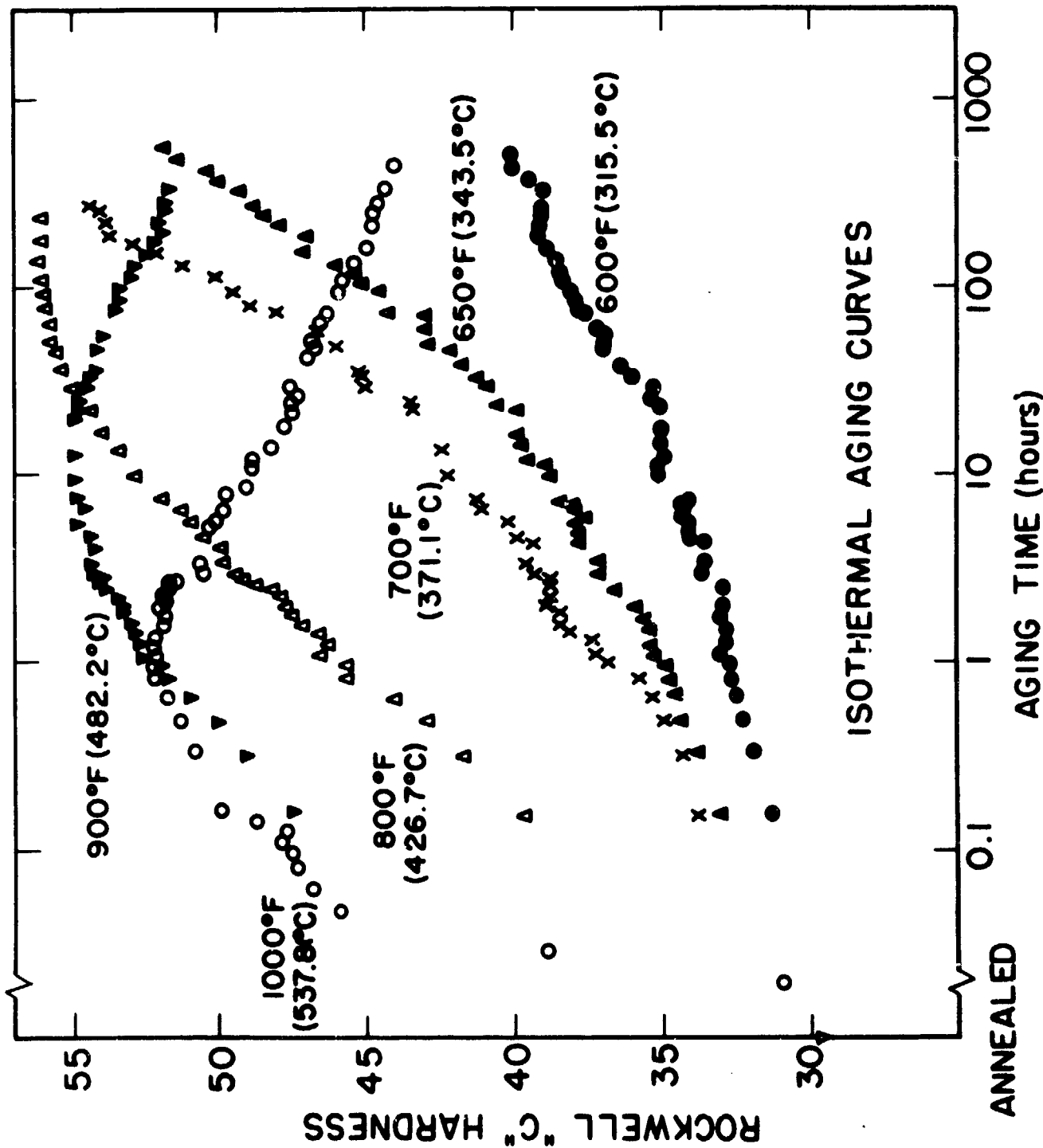
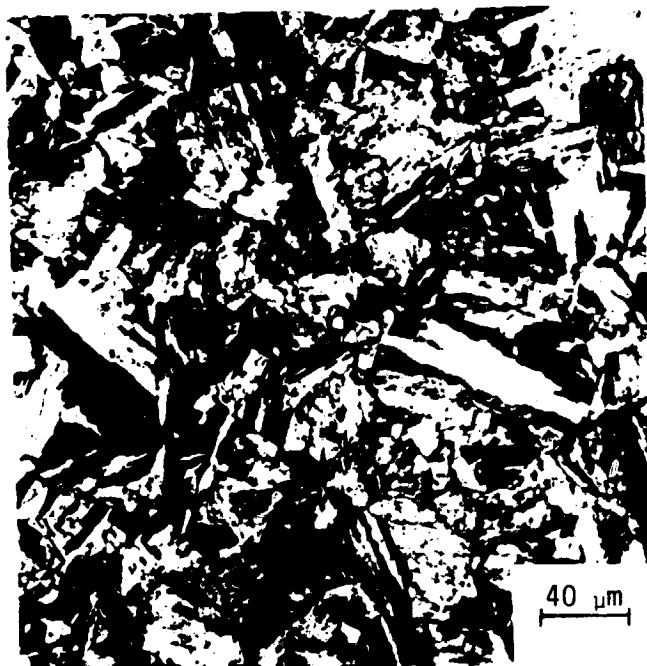


Figure 1 Hardness versus logarithm of time at temperature for some of the aging treatments used on the 18 Ni, 300 grade maraging steel.

of low temperature (low strength) must satisfy the plate thickness limitation of two inches for toughness specimen design. As will be seen in a later section of this report, the strengths attained by 3 hour treatments at 316°C (600°F) and 344°C (650°F) may be too low for valid plane-strain K_{IC} measurements. This can be seen by considering the empirical relation, $B = 2.5 (K_{IC}/\sigma_y)^2$ proposed by Brown and co-workers.^{40,41} As σ_y , the yield strength, is decreased, the specimen thickness, B, must be increased to satisfy this relationship. Progressively higher aging temperatures were examined so as to secure the lowest possible strength which can be successfully tested in this program. As will become evident in subsequent sections of this report, as yet, valid K_{IC} has not been measured for any of the low temperature conditions considered in this aging study.

C. Microstructure

Typical microstructures of the 18 Ni, 300 grade maraging steel are presented in Figure 2 as micrographs of polished and etched sections. The longitudinal or forging direction is vertical in Figure 2. The maraging steel was etched in Kalling's reagent, $CuCl_2$ and HCl in methanol and H_2O . This alloy exhibits very fine martensite laths shown in Figure 2a. These micrographs were taken from material aged for 3 hours at 482°C (900°F). The aged maraging steel exhibits a very fine precipitate structure within the martensite laths as is demonstrated. The prior austenite grain boundaries are shown in the TEM micrograph of a two stage replica taken from the polished and etched material shown in Figure 2b. A well developed Widmanstätten-like morphology is evident in Figure 2a. Floreen and Decker attribute the Widmanstätten-like structure to the martensitic transformation occurring upon cooling from the annealing temperature of 816°C (1500°F).⁴²

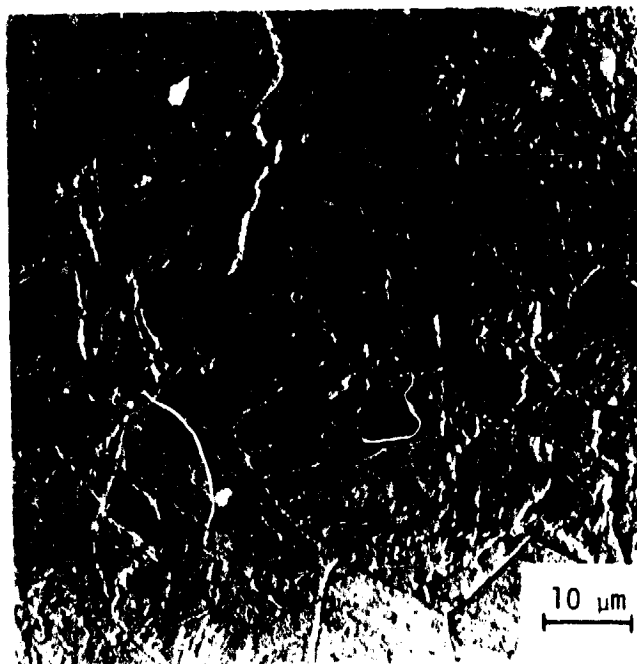


a.) Optical micrograph

Longitudinal
(Forging)
Direction



Transverse
Direction



b.) Transmission micrograph

Figure 2 Micrographs of polished and etched sections of 18 Ni, 300 grade maraging steel.

While at the annealing temperature, the structure is austenitic, face-centered cubic. The structure as shown in Figure 2 is apparently entirely body-centered cubic martensite. The etched micrographs show some evidence for the presence of second-phase impurity inclusions particularly in Figure 2a; however, the etchant used has obscured them to some extent. Much of the fine detail of the inclusions and their orientation with respect to the martensite laths will be examined with further use of TEM surface replication techniques. The prior austenite grain size as seen in Figure 2 is about 20-30 μm . A quantitative analysis to determine grain size is planned.

In order to define the exact nature of the impurity inclusions in the 300 grade maraging steel, a metallographic investigation was carried out. Polished, unetched metallographic sections were examined from each of three orthogonal directions, the axes being defined using ASTM E399-74 terminology⁴³ as the length, L (the major forging direction in this case), long transverse, T (the width), and the short transverse, S (the through thickness). As previously reported,¹ there are at least two types of second-phase impurity inclusions present in the 300 grade maraging alloy. Based upon their appearance in the optical microscope and comparison with descriptions from previous inclusion studies,⁹ these inclusions were tentatively identified as titanium carbonitrides ($\text{Ti}(\text{C},\text{N})$) and titanium sulfides (Ti_2S). The most prevalent shapes are shown in Figure 3. These micrographs are all taken from the LT plane. The inclusions that appeared as sections from cubes and sometimes rounded are pink in color and are believed to be $\text{Ti}(\text{C},\text{N})$. As shown in Figure 3, the two types of inclusions are often in contact with one another. The cubes did not appear to have been plastically deformed during the hot-forging operations. The elongated

and irregular inclusions appearing light gray in Figure 3 are similar to titanium sulfides (Ti_2S) and titanium carbides (TiC) observed in a previous investigation.⁹ Since the irregular inclusions are in the forging direction, they were undoubtedly plastically deformed during the hot-forging operations. Some of the inclusions have cracked, presumably due to the mechanical working. The cuboidal inclusions are usually less than 10 μm on edge. The elongated inclusions are frequently 20 μm long and usually less than 10 μm in width. The inclusions that are less than 1 μm in diameter will be examined with the aid of surface replica techniques and the TEM. As noted earlier, there is a fixed distribution of second-phase inclusion sizes in this heat of maraging steel which will not change with aging at the relatively low temperatures used in this program. Quantitative microscopy will be used to assess, by type, the size and spatial distribution of the second-phase impurity inclusions present in the 300 grade maraging steel.

To ascertain whether or not the preliminary identification of the second-phase impurity inclusions in the maraging alloy was correct, metallographic specimens were examined by using a scanning electron microscope (SEM) equipped with an X-ray energy-dispersive analyzer. Comparison of intensities of elemental characteristic X-rays from both of the inclusions and the matrix confirmed the postulated $Ti(C,N)$ and Ti_2S inclusion identifications. A representative group of micrographs taken of a cuboidal inclusion suspected to be a $Ti(C,N)$ is given in Figure 4. The cuboidal inclusion is richer in titanium than the matrix. A small amount of zirconium was found in the central region of this particle but was not clearly shown in an X-ray map. Unfortunately, no analysis can be made for carbon or nitrogen using this technique, but the strong signal from titanium together

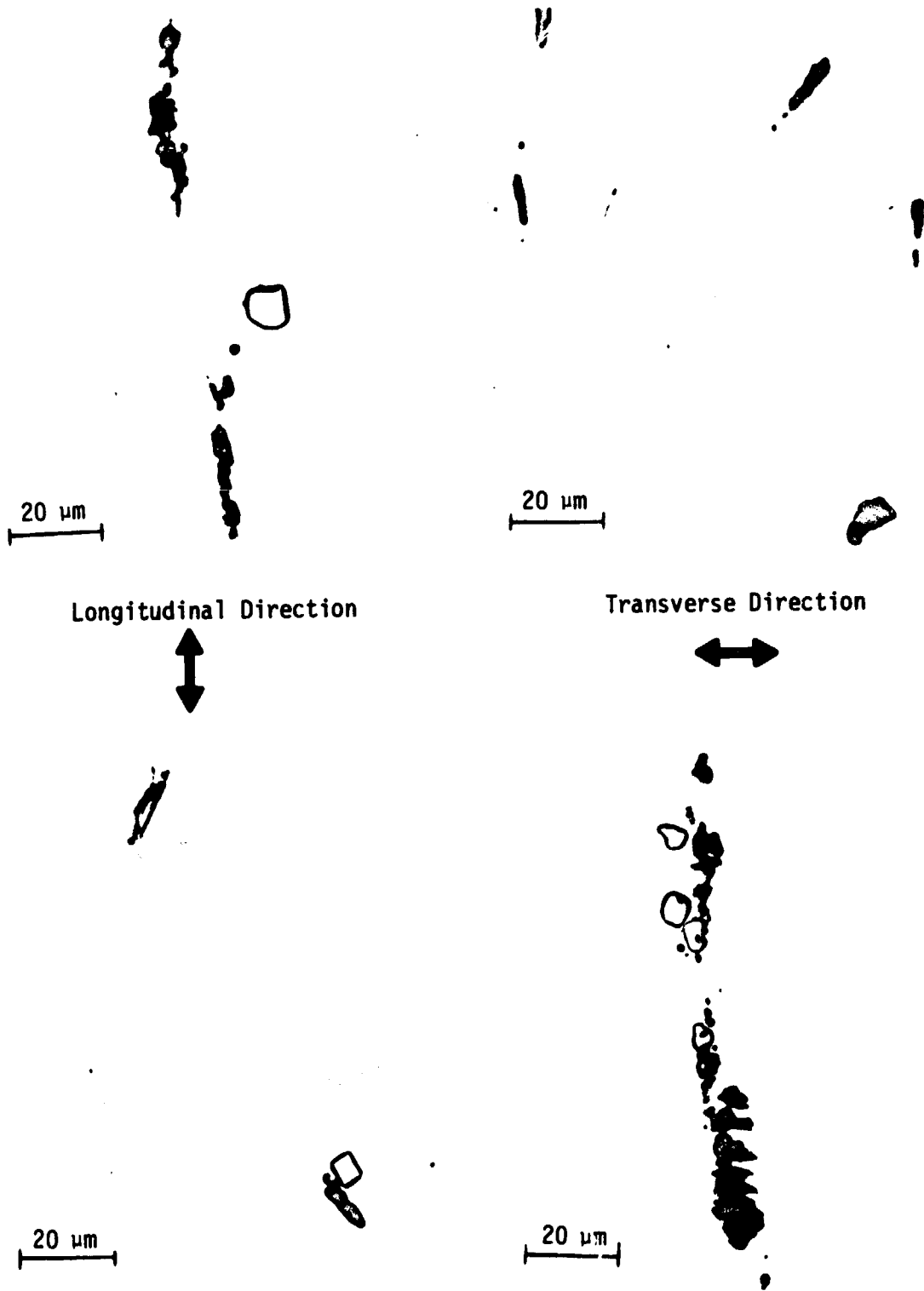
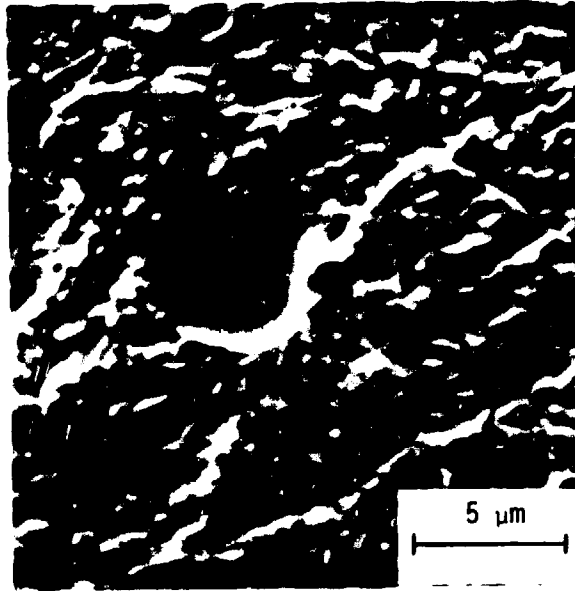
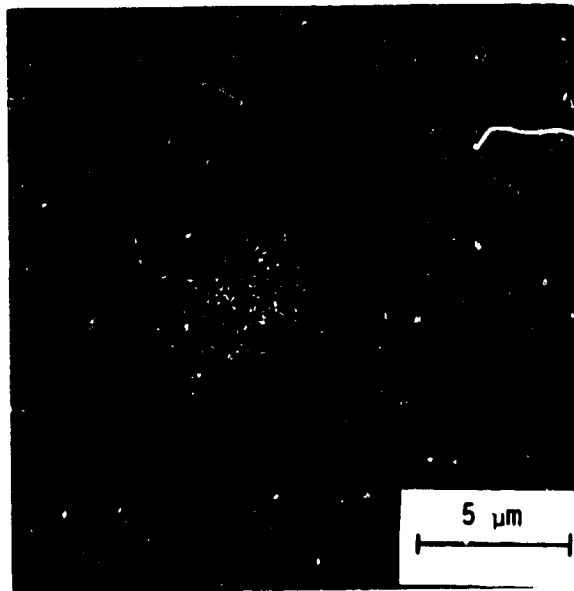


Figure 3 Optical micrographs of the most prevalent inclusions in the 18 Ni, 300 grade maraging steel.

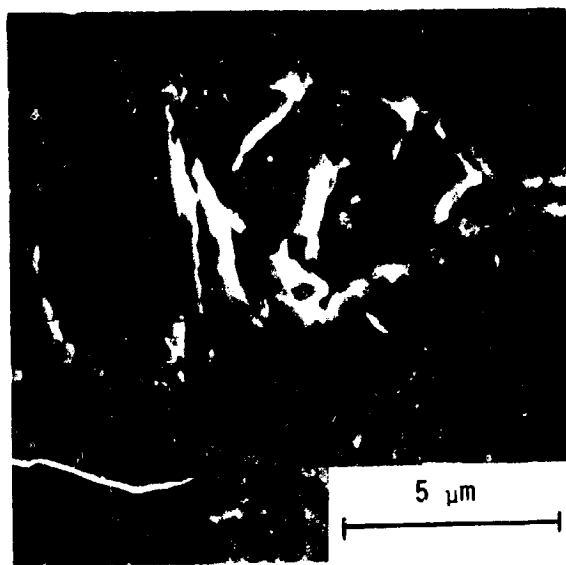


Back-scattered electron mode

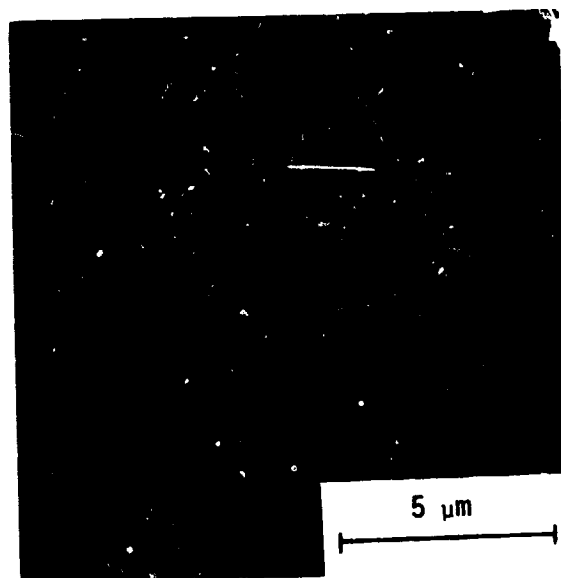


X-ray scan for titanium

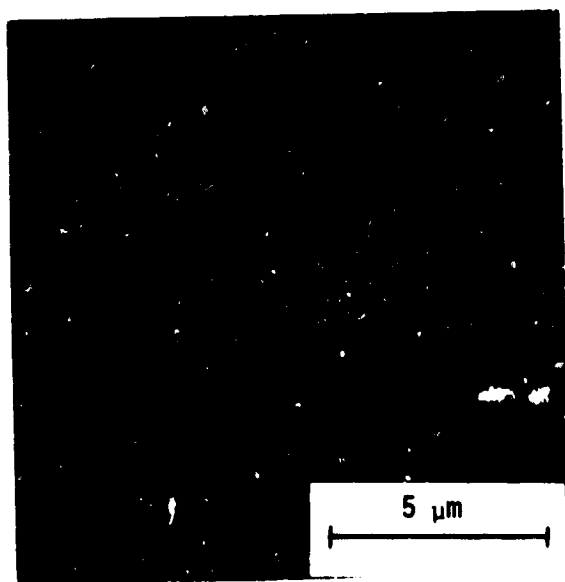
Figure 4 Scanning electron micrographs of Ti(C,N) inclusion in 300 grade maraging steel.



Back-scattered electron mode

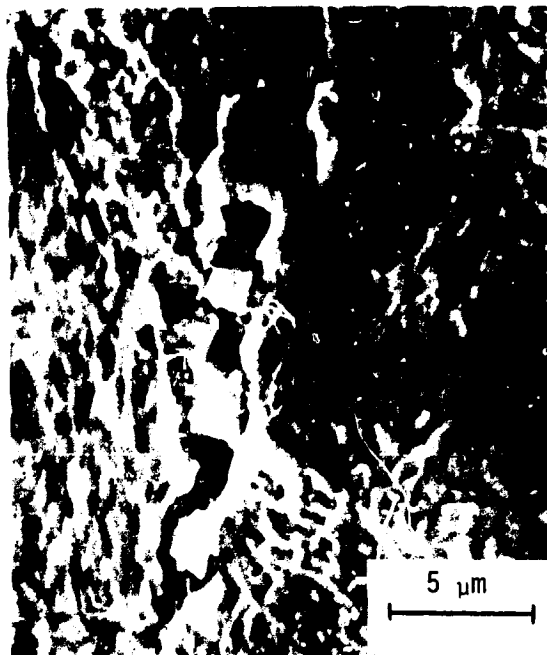


X-ray scan for titanium

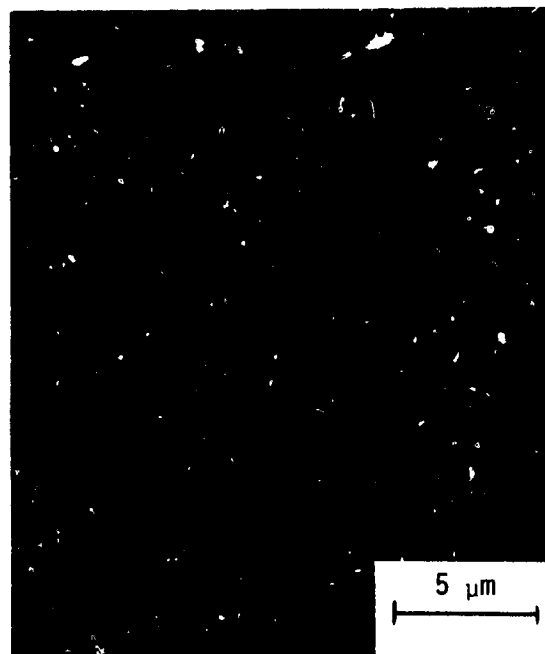


X-ray scan for sulfur

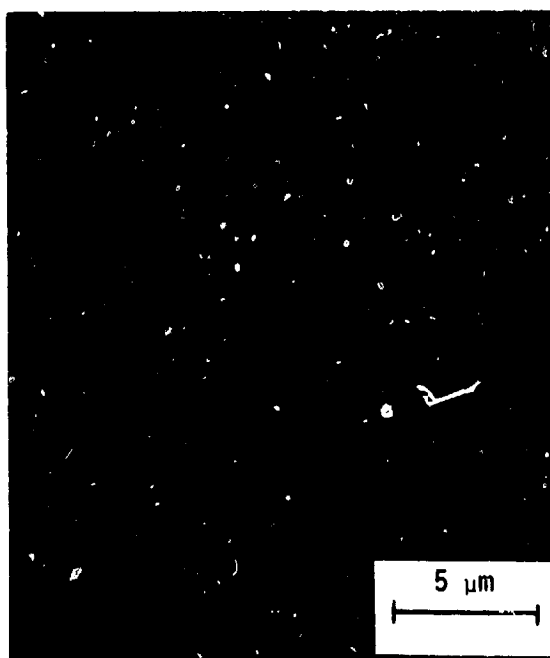
Figure 5 Scanning electron micrographs of an irregular shaped Ti_2S inclusion in 300 grade maraging steel



Secondary electron mode



X-ray scan for titanium



X-ray scan for sulfur

Figure 6 Scanning electron micrographs of an elongated Ti_2S inclusion in 300 grade maraging steel

with their optical morphology clearly indicates that the cuboidal inclusions in the 300 maraging alloy are titanium carbonitrides.

A similar procedure was used for analyzing the irregular gray inclusions. In this case, however, the inclusions were richer than the matrix in both titanium and sulfur. At approximately 0.005 weight percent, the bulk sulfur concentration in the matrix is too low to produce a measurable characteristic X-ray signal for sulfur. Figures 5 and 6 are examples of representative micrographs of titanium sulfide inclusions in the 300 grade maraging steel. Figure 5 is from a highly irregular shaped inclusion which is clearly cracked. Figure 6 is from a Ti_2S inclusion which is more regular but also elongated and cracked. Both these irregular shapes are rich in sulfur and titanium. Included are photomicrographs taken in the secondary and back-scattered electron modes and from the same area are elemental X-ray scans for Ti and S. The detection of both titanium and sulfur in the inclusions together with their optical appearance and previous investigations indicate that the irregular gray inclusions are titanium sulfides.

In an attempt to isolate the inclusions which are detrimental to the fracture toughness, a similar procedure is planned for examination of inclusions in situ from K_{IC} fracture surfaces.

MECHANICAL PROPERTIES

In this investigation the mechanical properties of the 300 grade maraging steel were characterized using tensile tests, fatigue precracked Charpy impact tests, and plane-strain fracture toughness, K_{Ic} tests. All three types of tests were conducted at room temperature (20°C or 68°F). These properties were examined at several strength levels in this heat of 18 Ni, 300 grade maraging steel. Before the results of these tests are presented, the techniques used and problems encountered will be described.

To establish an initial measure of the magnitude of the strength-toughness trend in the 300 grade maraging alloy, fatigue precracked Charpy impact tests were performed. Standard Charpy impact specimens were cut from the annealed plate and prepared from the longitudinal direction, the V-notch lying in the forging plane. The crack was designed to propagate in the transverse direction in the plate. The notches were machined sharp so that a subsequent fatigue precrack could start more easily on a single plane. To establish an extensive range in strength, the machined impact specimens were aged at eight different temperatures. The specific treatments and resulting strengths will be given in the next section of this report. Once aged, each specimen was fatigue precracked to a crack depth to specimen thickness ratio, of between 0.3 and 0.5. Fatigue precrack propagation was observed on the prepolished surface of the Charpy with a low power microscope. A three-point bending fixture was designed for precracking the standard size Charpy specimens. Care was taken to maintain reasonable crack-front straightness.

Once precracked, the specimens were tested at room temperature in impact on a 240-ft-lb (325 joules) impact machine. Energy absorbed, W , in

impact and average crack length were recorded. The area carrying load, A , in impact was computed using the standard trapezoidal rule for estimating area under the fatigue crack front which had a usual amount of curvature associated with it. From work reported in the literature, estimates of K_{IC} were determined from these fatigue precracked Charpy impact tests and correlated to K_{IC} through the total energy per unit area, W/A , involved in fracture.⁴⁴ It should be noted that there has not been any claim made that precracked Charpy estimated toughness data satisfy the criteria outlined in ASTM standard E399-74 for valid K_{IC} measurements.⁴³

Tensile properties at all strength levels considered and plane-strain fracture toughness properties at selected strength levels were determined at Carnegie-Mellon University. Selected low strength fracture toughness properties will be determined at the NASA Lewis Research Center. All testing will be performed at room temperature, 20°C (68°F). Final selection of the strength levels to be tested at the two locations will be based upon ASTM E399-74 requirements for valid plane-strain K_{IC} testing.⁴³ For the high and intermediate strength levels, 1.88 cm (0.75 inch) and 2.54 cm (1.0 inch) thick compact tension specimens are being used. In the lowest strength level for which a valid K_{IC} can be measured, 5.08 cm (2.0 inch) thick three-point bend K_{IC} specimens are to be used. The design and relative size variation in the tensile, standard Charpy, 1.88 cm (0.75 inch) and 2.54 cm (1.0 inch) compact tension, and 5.08 cm (2.0-inch) three-point bend K_{IC} specimens are shown in Figure 7. There are additional fatigue precracking problems which must be resolved prior to determining the final range of strength which can be matched with valid K_{IC} data. Fatigue in the 300 grade maraging steel will be discussed in a separate section of this report.

To determine tensile properties and flow curves as a function of strength level, 6.25 mm (0.25 inch) diameter, smooth cylindrical tensile specimens were used. A linear variable differential transformer (LVDT) extensometer with a 2.54 cm (1.0 inch) gage length was used to record the specimen extension up to the point of maximum load where necking begins and strain becomes localized. The gain and phase angle between the primary and secondary signals of the LVDT were adjusted so that a maximum output signal would be attained. The details of the calibration technique for the LVDT were developed by Shannon.⁴⁵ Load and extension were automatically recorded up to the maximum load. Beyond the maximum load and the onset of necking, the minimum diameter was measured with a point micrometer and the corresponding load was recorded several times up to fracture. Each measurement after necking constituted a datum point for construction of the flow curve for that strength level.

The fracture strain was calculated from the minimum diameter of the fractured specimen. Triplicate tests were run at each strength level and statistical analysis applied to the data. The measure of strain used throughout this report is the diametral strain (ϵ) which is defined in Equation (1).

$$\epsilon = 2 \ln (d_0/d_f) \quad (1)$$

where

d_0 = initial specimen diameter

and

d_f = instantaneous specimen diameter.

The 0.2% offset yield strength (σ_y) and the ultimate tensile strength (UTS) were determined directly from the load extension record.

Using the load-extension record and the data taken after the point of

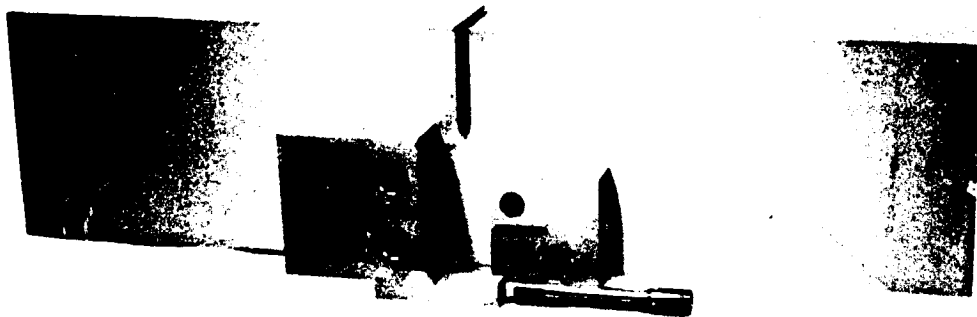


Figure 7 Smooth, round (0.252-inch diameter) tensile, standard Charpy, 0.75-inch and 1.0-inch thick compact tension specimens and 2.0-inch thick 3-point bend specimen.

maximum load, the true stress-plastic strain curves at various strength levels were determined. As noted by Bridgman,⁴⁶ there is a region of hydrostatic tension in the necked region of a tensile specimen. To account for the component of hydrostatic stress, the true stress data after necking was corrected using the Bridgman correction.⁴⁶ The flow stress (σ) was calculated by multiplying the true stress by the Bridgman correction factor (F) for cylindrical specimens. The Bridgman correction factor is given in Equation (2).

$$F = 1/\{(1 + 2R/a) \ln (1 + a/2R)\} \quad (2)$$

where

a = the minimum radius of the specimen in the necked region

and

R = the radius of curvature of the neck.

The correction factor is a function only of the neck geometry. Bridgman showed that a plot of a/R as a function of strain was linear up to strains of unity for a wide variety of steels. For this investigation, plastic strains no greater than about 1.5 would be expected based upon preliminary data. A linear least square regression line for Bridgman's data up to a plastic strain of 1.5 was prepared. Although the scatter in Bridgman's data is extensive, the linear fit of a/R to the plastic strain (ϵ) is quite good over this range of strains. The computed fit is given in the following Equation (3).

$$a/R = -0.026 + 0.800\epsilon \quad (3)$$

According to this relationship, a/R would be negative below plastic strains of about 0.03. This value is in excellent agreement with the uniform plastic strains for the maraging steel. Since no neck exists with uniform

plastic strain by definition, the true stress is considered to be the flow stress. Above strains of 0.03, Equations (2) and (3) are used to calculate the Bridgman correction factor and the flow stress.

With the aid of a computer program⁴⁷ written to calculate the plastic strain, true stress, and flow stress for each datum point from the load, extension and minimum diameter data, flow curves can be determined. An empirical fit is made relating the flow stress (σ) to the plastic strain (ϵ) using Equation (4)

$$\sigma = \sigma_0 + A\epsilon^m \quad (4)$$

where

σ_0 , A and m = constants determined by a least squares regression technique.

It has been found in an analysis of several of the data sets for the 300 grade maraging steel in this investigation that the fit of the data to Equation (4) is significantly better than that achieved by relating flow stress and plastic strain using Equation (5).

$$\sigma = K\epsilon^n \quad (5)$$

where

K and n = constants determined by a least square regression, and σ_0 equals zero.

The stresses calculated from the regression analysis using Equation (4) were usually within 1 or 2 percent of the experimental values. Figure 8 shows an example of the engineering stress, true stress, and Bridgman corrected true stress (flow curve) plotted against the true plastic strain for room temperature tests on the 300 grade maraging steel aged for 3 hours at 399°C (750°F).

The plane-strain fracture toughness tests were performed at room tem-

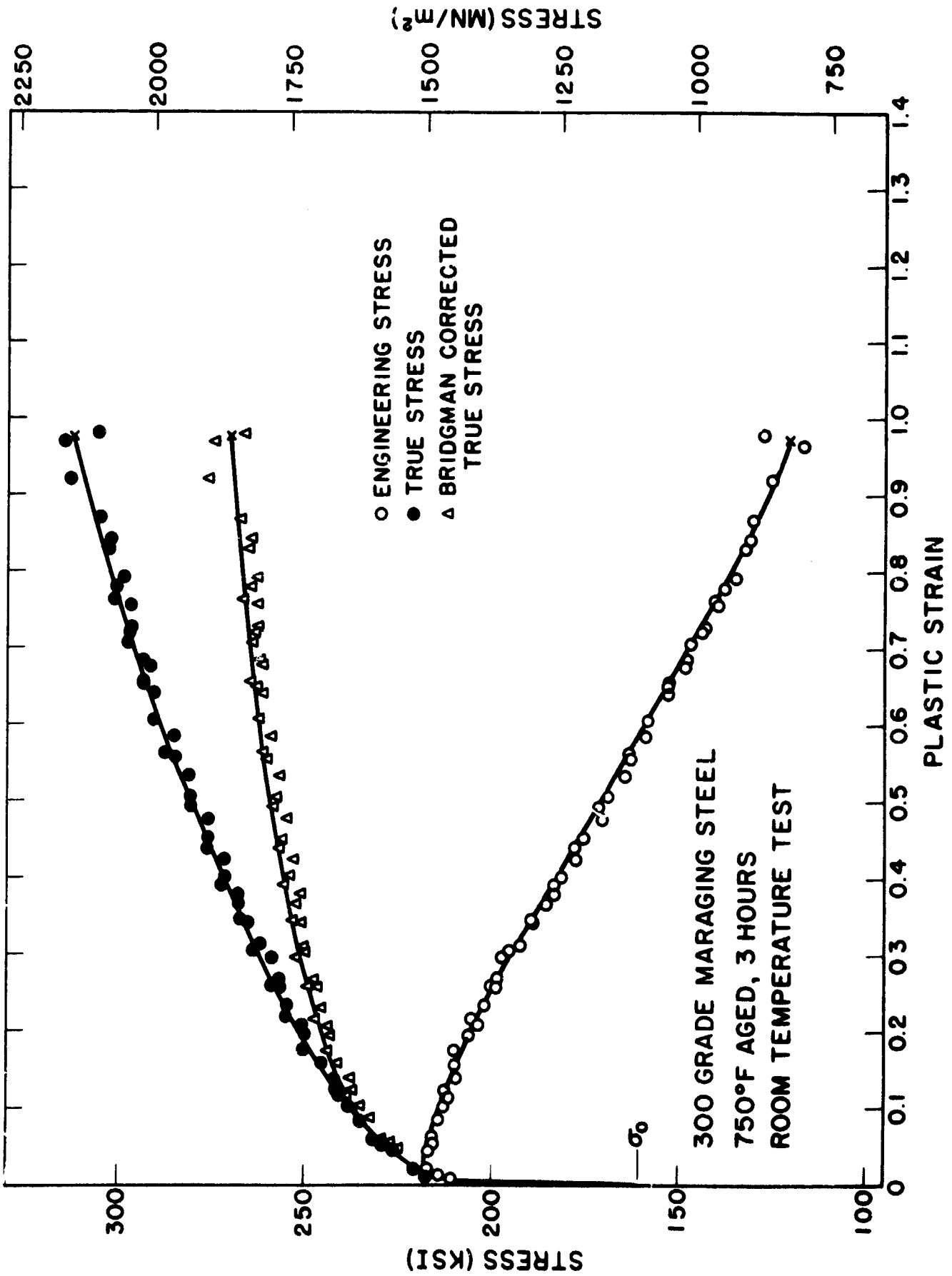


Figure 8 Example engineering, true, and Bridgman corrected true stress-strain curves.

perature, 20°C (68°F). Standard compact tension specimens⁴³ of 1.88 cm (0.75 inch) thickness were used for the 300 grade maraging steel aged for 3 hours at 427°C (800°F), 482°C (900°F), and 538°C (1000°F). The 1.88 cm (0.75 inch) thick specimens were also used for the 100 hour, 427°C (800°F) aging treatment. A 2.54 cm (1.0 inch) thick compact tension specimen was used for the slightly lower strength material resulting from a 3 hour treatment at 399°C (750°F). Displacement at the mouth of the machined notch in the compact tension specimen was monitored with an LVDT clip gage seated in knife edges that were attached to the specimen. The knife edge design is the same as that used by Van Stone, Low, and Shannon.⁴⁸

A. Mechanical Test Results

The mechanical properties of the 18 Ni, 300 grade maraging steel were determined at 20°C (68°F). The number of aging conditions (strength levels) considered were not identical for the tensile, fatigue precracked Charpy, and K_{Ic} tests. Some of the lower strength levels for which conventional tensile properties were determined cannot be tested in a valid manner for plane-strain fracture toughness due to the ASTM E399-74 thickness requirements.⁴³ The initial choice of aging temperatures was made without knowledge of the extensive range in fracture toughness that has evidently resulted. Additionally, at some of the intermediate strength levels the conditional plane-strain fracture toughness values (K_Q) measured were invalid due to a fatigue precrack problem which will be explained in the next section. Until this problem is resolved the plan to use 5.08 cm (2.0 inch) thick 3-point bend specimens cannot be implemented.

The tensile properties were determined for longitudinal tensile specimens. The tensile specimens were aged for 3 hours at 316°C (600°F), 329°C (625°F), 344°C (650°F), 371°C (700°F), 399°C (750°F), 427°C (800°F),

482°C (900°F), and 538°C (1000°F). The tensile testing program also included the solution treated condition and the maximum strength level attained by aging for 100 hours at 427°C (800°F). In all, the tensile properties were determined for 10 different strength levels of the 300 grade maraging steel. The fatigue precracked Charpy impact tests were performed for all of the above aging conditions except for the solution treated and 100 hour treatment at 427°C (800°F). The plane-strain fracture toughness was determined from 1.88 cm (0.75 inch) and 2.54 cm (1.0 inch) thick compact tension specimens in the LT orientation (crack plane perpendicular to the plate longitudinal direction and crack propagation in the transverse direction). The fatigue precracked Charpy specimens were also of the LT orientation. Specimens aged for 3 hours at 427°C (800°F), 482°C (900°F), and 538°C (1000°F); and 100 hours at 427°C (800°F) were of the 1.88 cm (0.75 inch) thick compact tension specimen design. The 1.88 cm (0.75 inch) and 2.54 cm (1.0 inch) thick specimens were used unsuccessfully to measure K_{Ic} for material aged for 3 hours at 399°C (750°F).

The tensile, fatigue precracked Charpy estimated toughness, and limited fracture toughness properties of the 18 Ni, 300 grade maraging alloy are given in Table II. These data represent the averages and standard deviations of multiple tests except where otherwise noted. The specimen measurements and other details of the individual toughness tests are given in Appendix A.

It can be seen from Table II that the aging treatments used have established an extensive range of strength levels. Based upon a comparison of yield strengths, the 100 hour, 427°C (800°F) material is about 1350 MN/m² (196 ksi) stronger than the solution treated material. A more realistic strength range comparison should be considered. That is, one for which

TABLE II

MECHANICAL PROPERTIES OF 18 Ni, 300 GRADE MARAGING STEEL

Room Temperature Tests

(Data indicates the mean \pm one standard deviation)

Aging Temperature $^{\circ}\text{C} (^{\circ}\text{F})$	Aging Time (hrs.)	σ_y 0.2% Yield Strength (ksi) (a)	Ultimate Tensile Strength (ksi) (a)	Fracture Strain	Precracked Charpy Estimated K_{Ic} ($\text{ksi}/\sqrt{\text{in.}}$) (b)	K_{Ic} ($\text{ksi}/\sqrt{\text{in.}}$) (b)
Solution Treated	-	104.1 \pm 0.0	145.2 \pm 0.2	1.558 \pm 0.007	-	-
316 (600)	3	129.0 \pm 0.7	159.9 \pm 0.3	1.363 \pm 0.004	347.6 \pm 10.5	-
329 (625)	3	137.6 \pm 0.7	164.2 \pm 0.1	1.331 \pm 0.016	337.8 \pm 6.1	-
344 (650)	3	147.1 \pm 0.9	171.9 \pm 0.9	1.260 \pm 0.005	313.5 \pm 6.8	-
371 (700)	3	157.9 \pm 1.5	182.6 \pm 1.0	1.207 \pm 0.020	280.2 \pm 16.6	-
399 (750)	3	198.3 \pm 0.4	217.8 \pm 0.5	0.956 \pm 0.030	131.9 \pm 4.1	(c)
427 (800)	3	225.1 \pm 0.4	239.1 \pm 1.9	0.778 \pm 0.022	94.2 \pm 3.0	96.6 \pm 7.0
482 (900)	3	268.8 \pm 1.3	278.9 \pm 1.0	0.742 \pm 0.010	91.2 \pm 3.8	78.2 \pm 0.4
538 (1000)	3	246.3 \pm 0.4	259.8 \pm 1.6	0.635 \pm 0.020	90.4 \pm 2.7	66.7 \pm 1.8
427 (800)	100	299.6 \pm 1.5	308.4 \pm 0.7	0.468 \pm 0.021	-	50.9 \pm 0.2

(a) 1 ksi = 6.9 MN/m²(b) 1 $\text{ksi}/\sqrt{\text{in.}}$ = 1.1 MN/m^{3/2}

(c) These results are invalid for reasons given in the text and are listed in TABLE IV.

valid K_{IC} measurements might conceivably be made based upon the plate thickness limitation of two inches. Assuming the 371°C (700°F) aging treatment to produce the lowest strength for valid K_{IC} , a variation in strength of about 978 MN/m² (142 ksi) is available for investigation. With increasing strength and/or overaging, the valid K_{IC} data show a decrease of nearly 55 MN/m^{3/2} (50 ksi√in). From a consideration of the results attained thus far, both valid and invalid, it is estimated that the range in valid plane-strain fracture toughness that this investigation will examine is between 99 and 110 MN/m^{3/2} (90 and 100 ksi√in).

As expected, the fatigue precracked Charpy impact, W/A, data correlated to fracture toughness, K_Q , shows an extensive property variation with strength. Figure 9 is a plot of the data given in Table II and quite clearly the inverse relationship between strength and this crude measure of toughness is evident. It should be noted that the ability of the fatigue precracked Charpy impact test to estimate K_{IC} rapidly decreases as the strength decreases. The energy required to break a low strength Charpy is expended mainly in the gross plastic deformation of the material rather than in crack propagation. The plastic flow associated with shear lip formation increases as strength decreases since the Charpy thickness is inadequate to maintain plane-strain constraint at the crack tip. These data do, however, illustrate the strength-toughness trend necessary for this program.

A similar plot of strength versus toughness is given in Figure 10. In this figure are plotted valid K_{IC} against the 0.2% offset yield strength data available to date. These data are averages of at least three tests per condition. The error bars indicate the range of plus and minus one standard deviation (68 percent confidence limits). Where error bars are not shown, the standard deviation is smaller than the point representing the average

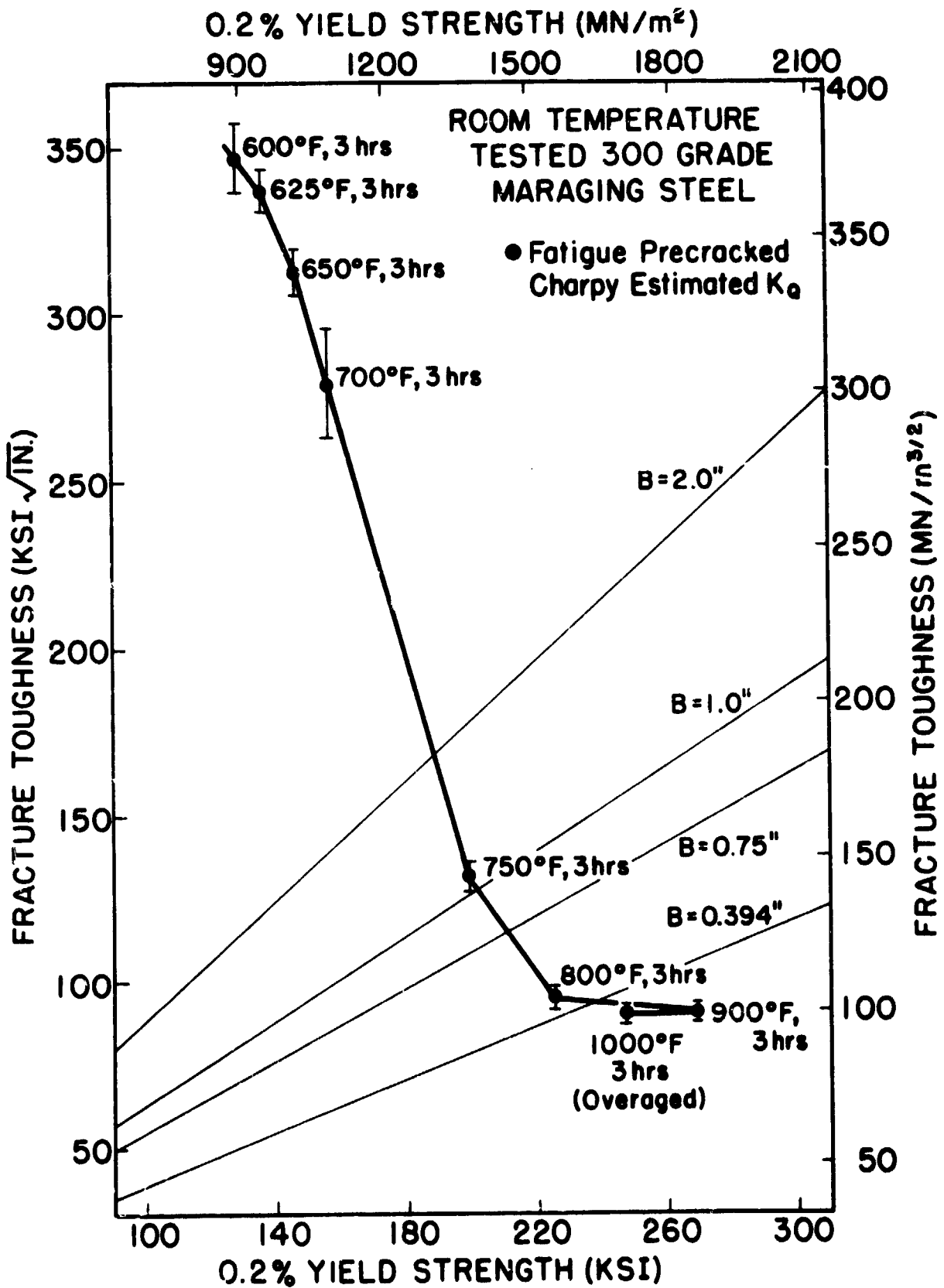


Figure 9 Fatigue precracked Charpy estimated K_Q as a function of strength for room temperature impact tests.

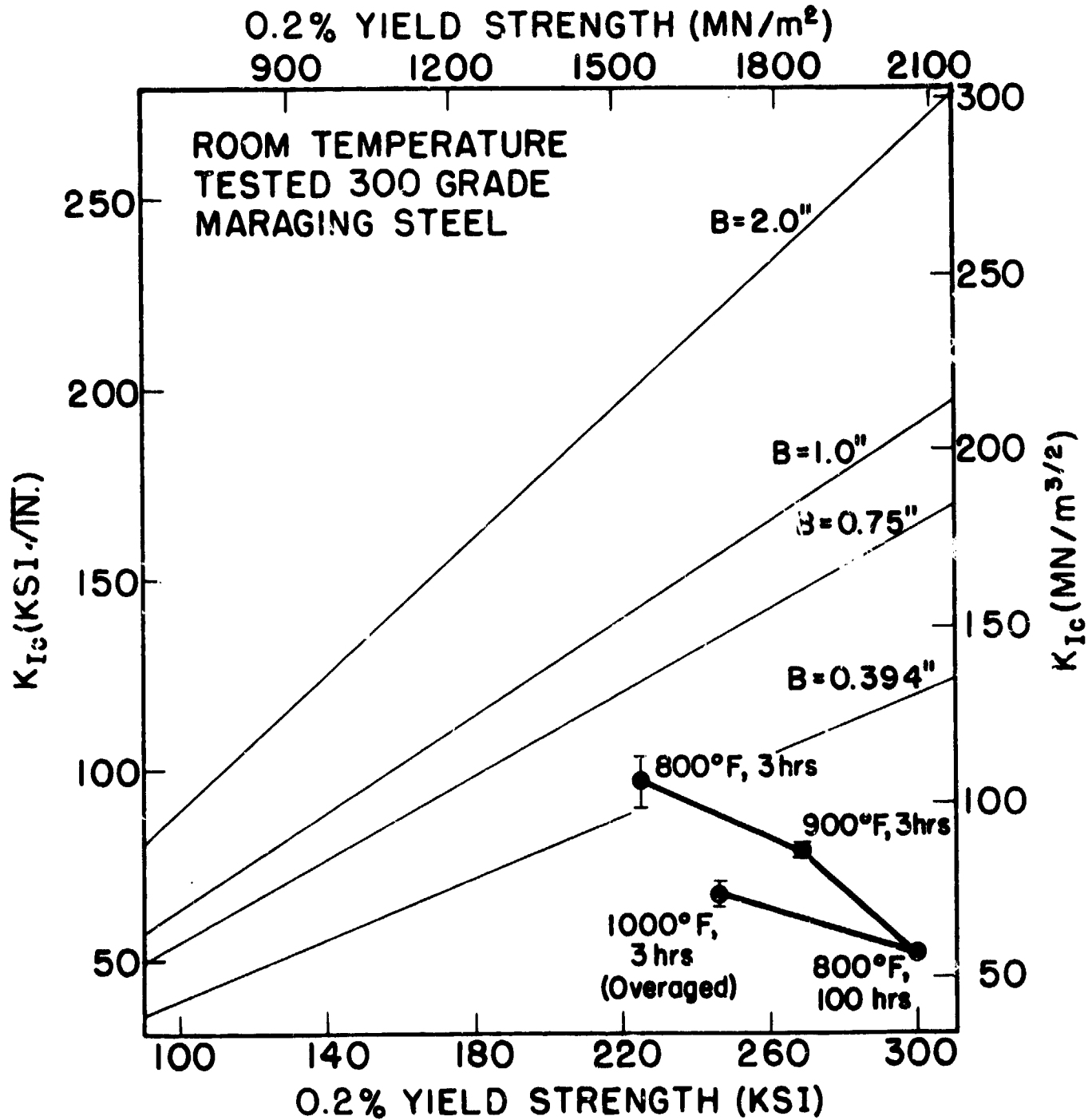


Figure 10 Valid K_{Ic} fracture toughness of variously strengthened 18 Ni, 300 grade maraging steel at 20°C (68°F) determined using 0.75-inch thick compact tension specimens.

value. The invalid K_{IC} data for the 399°C (750°F) aging condition are not shown in Figure 10 since the scatter in the results would only serve to confuse the trend. A detailed explanation for the degree of scatter of the invalid toughness data for the 399°C (750°F) aging condition will be given in the next section of this report. It is also indicated in Figure 9 that toughness decreases with increasing strength and with overaging. In other words, at a yield strength of about 1725 MN/m² (250 ksi) the underaged material is expected to be about 22 MN/m^{3/2} (20 ksi√in) tougher than the overaged material. A possible explanation for the continued decrease in toughness with overaging is related to the size of overaged precipitates and their role in the void coalescence process. Details of this explanation and some fractographic evidence will be presented in the fractography section of this report. It is interesting to note that the tensile fracture strain data decrease with increasing strength and/or overaging in a similar fashion to the toughness data. This trend provides at best a rough indication that deformation in the tensile and K_{IC} specimens might be comparable.

The tensile flow curves of the 18 Ni, 300 grade maraging steel aged to the strength levels given in Table II are plotted in Figure 11. The symbols shown are experimental data points from multiple tensile specimens for each strength level and the solid curves are the results of the least squares regression empirical flow curves of the form given previously in Equation (4). Use has been made of a different symbol for each flow curve for visual aid purposes only. The fitted curves are terminated at the average fracture strain given in Table II and indicated by a small "x." It should be noted that the tensile flow curves for the solution treated, the 329°C (625°F) and the 344°C (650°F) conditions were not included in Figure 11 since they were only slightly different than the 316°C (600°F) age.

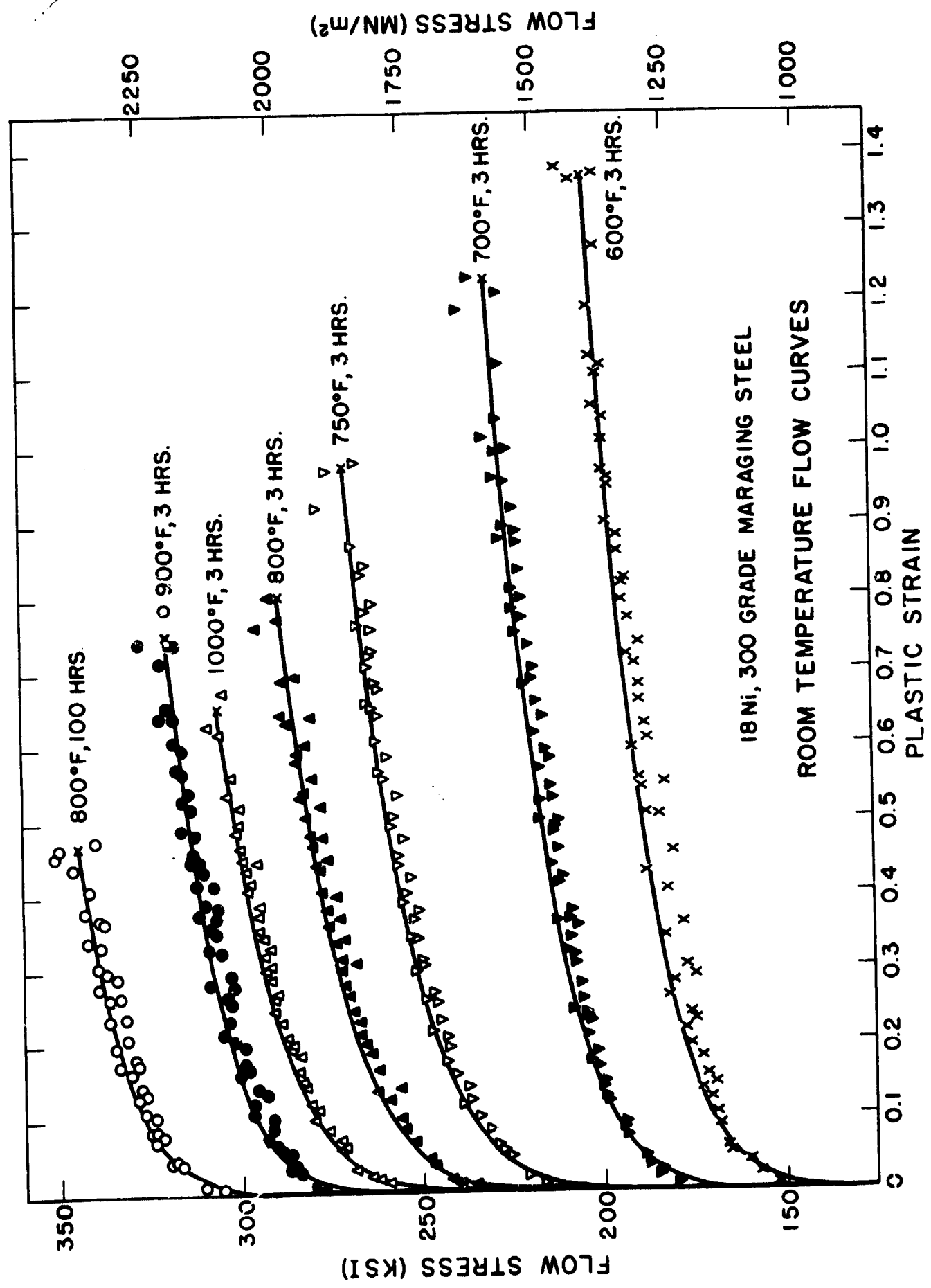


Figure 11 Room temperature tensile flow curves of variously aged 300 grade maraging steel. Solid lines are the result of the regression analysis.

With all of the curves included, the additional data points and regression lines would only serve to confuse the trend in flow properties that Figure 11 is intended to illustrate. Some of the data points measured from the load-extension test records are not shown in Figure 11 but were used in the regression analysis. The data not shown is only for strains up to about 0.0 and again this is for purposes of clarity in the figure. The constants σ_0 , A , and m from the empirical flow curves at each strength level are listed in Table III. The statistical significance, which is a measure of the goodness of fit of the curves to the data is also given in Table III. The statistical significant value was calculated using a paired t- test⁴⁹ by comparing the experimental flow stress with that calculated from the empirical flow curve at a given plastic strain. This was done for each strength level considered. The significance can be interpreted as the probability that the experimental flow curve data and the empirical flow curve values belong to the same population. The fit of the data to this form of flow curve is excellent for all strength levels examined. The fit of the data to the empirical form given in Equation (5) is in all cases not as good as with that in Table III but it too would be an acceptable alternative.

In recent studies^{4,32} it has been found, not without uncertainty, that the event of void initiation by either inclusion cracking or inclusion matrix interface separation requires some plastic deformation to have occurred. The possible requirement for plastic deformation will be examined in this investigation at each strength level considered. If plastic deformation is necessary then the σ_0 values which have been calculated may have added significance in a possible correlation between strength (stress) and void initiation. Since σ_0 is an apparent elastic limit, it delineates the transition from elastic to plastic deformation. Care must be taken when using σ_0

TABLE III

FLOW CURVES OF 300 GRADE MARAGING STEEL AT VARIOUS STRENGTH LEVELS

FIT TO THE FORM $\sigma = \sigma_0 + A\epsilon^m$ WHERE σ IS THE FLOW STRESS

AND ϵ IS THE TRUE PLASTIC STRAIN

Room Temperature Tests

Solution Treated	Aging Temperature °C (°F)	Aging Time (hrs.)	Room Temperature Tests		m	Level of Significance (%) (b)
			σ_0 (ksi) (a)	A (ksi) (a)		
		-	57.4	132.9	0.131	97.0
316 (600)		3	82.8	115.8	0.122	97.5
329 (625)		3	99.1	106.8	0.138	97.8
344 (650)		3	110.6	101.5	0.139	97.4
371 (700)		3	124.3	103.0	0.152	98.8
399 (750)		3	160.3	110.8	0.162	99.2
427 (800)		3	191.7	100.8	0.177	98.8
482 (900)		3	236.0	87.7	0.165	>99.9
538 (1000)		3	212.4	100.6	0.176	98.6
427 (800)		100	261.0	93.7	0.152	>99.9

(a) 1 ksi = 6.9 MN/m²

(b) Determined using a t-test on paired data

since this value is dependent upon the strain resolution of the LVDT used in the tensile test.

The rate of strain hardening was calculated from the empirical flow and is given as $\partial\sigma/\partial\epsilon = mA\epsilon^{m-1}$. When plots of $\partial\sigma/\partial\epsilon$ versus ϵ are constructed for the 300 grade maraging steel in all of the strength levels considered in Table III, the curves cannot be distinguished from one another. The strain hardening behavior for the 300 grade maraging steel is independent of strength level over a yield strength range of about 1350 MN/m^2 (196 ksi). This could be a very important factor to consider when material flow properties are related to void growth as a function of strength. Because of the excellent fit of the empirical flow curves, the calculated $\partial\sigma/\partial\epsilon$ values are considered accurate measures of the material's strain hardening behavior.

B. Fatigue Precracking Behavior

The value of K_{IC} , the critical plane-strain stress-intensity factor, is an important measure of toughness. It is a material constant, it can be used in design to calculate a critical crack size for a given applied stress, and it can be determined experimentally using suitably designed laboratory specimens and tests as described above. The K_{IC} value is calculated by equations established on the basis of linear elastic stress analysis. The validity of the determination of K_{IC} value by this method depends upon the establishment of a sharp crack condition at the tip of the fatigue crack. The sharp crack must, under severe tensile constraint, produce a state of stress near the crack front that approaches triaxial plane-strain, and the crack-tip plastic zone must be small compared with the crack size and specimen thickness.

Although fatigue precracked Charpy impact specimens provide only a fair

to poor approximation of the above conditions dependent upon the strength level, use of precracked Charpies was made merely to establish a quick and cheap measure of strength-toughness trend. The fatigue precracking of both Charpy and compact tension K_{IC} specimens at Carnegie-Mellon University was performed on a 900 kg (2000 lb) Sonntag Universal fatigue testing machine. Unless otherwise noted, fatigue precracking was performed at room temperature, 20°C (68°F) in air. All specimens were fatigued in the aged condition in which they were to be subsequently tested. All specimens that were prepared in this system for purposes of measuring impact W/A or K_{IC} were precracked at a maximum stress intensity range in fatigue (ΔK) of about 22 MN/m^{3/2} (20 ksi√in). This corresponds to about 40 percent of K_{IC} in the least tough condition. Unless otherwise noted, fatigue was performed at 30 cycles per second (30 Hz). With a ΔK of 60 percent of K_{IC} permitted by ASTM E399-74, the facility satisfies acceptable standards.⁴³

The 1.88 cm (0.75 inch) thick compact tension specimens aged at temperatures above 399°C (750°F) were precracked and tested resulting in the valid K_{IC} data listed in Table II. In the specimens aged at temperatures above 399°C (750°F) where valid K_{IC} resulted, the maximum load and fast fracture occurred at specimen deflections less than the 5 percent offset secant deflection. In the specimens aged for 3 hours at 399°C (750°F), however, the maximum load (P_{max}) exceeded the 5 percent offset secant load (P_5) by anywhere from 12 to 122 percent depending on the particular test. Fast fracture occurred at a specimen deflection much greater in all cases than that of the 5 percent offset secant. The tests were considered invalid because a specimen whose maximum load exceeds the 5 percent offset secant load by more than 10 percent, would fail to meet the requirements of

the ASTM Test Method.⁴³ These invalid tests included 1.88 cm (0.75 inch) and 2.54 cm (1.0 inch) thick compact tension K_{Ic} specimens. The 1.88 cm (0.75 inch) thick specimens were used first to determine if the smaller size specimen was of sufficient thickness to yield valid toughness data at slightly lower strength levels. Once invalid data resulted from duplicate 1.88 cm (0.75 inch) thick specimens, the 2.54 cm (1.0 inch) thick specimens were aged at 399°C (750°F), precracked, and tested. Again these results were invalid for what appeared to be the same reasons.

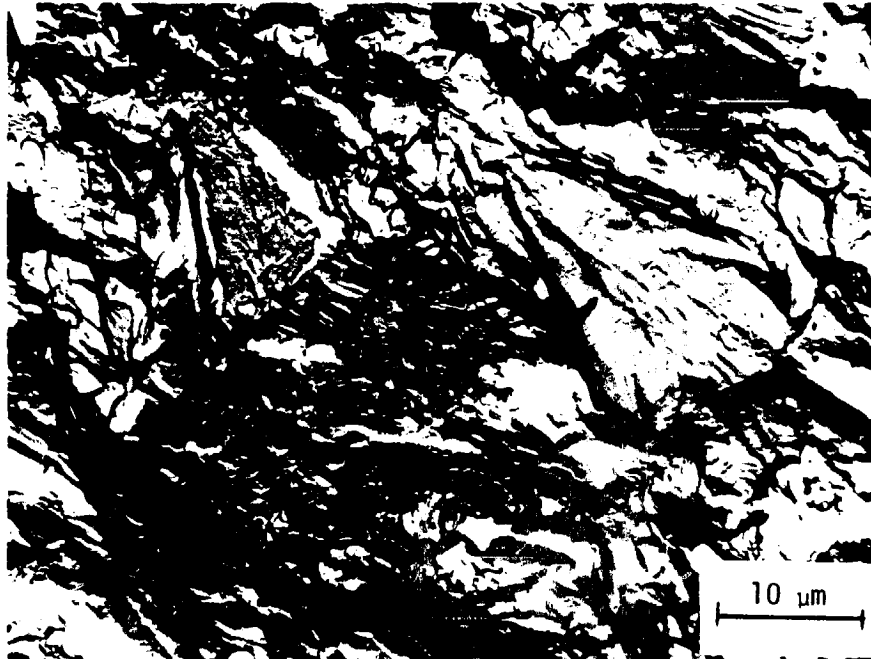
Visual observation of the region around the crack-tip in each of the invalid compact tension specimens during the course of testing revealed the formation of an extensive plastic zone and cracks forming shortly thereafter at what appeared to be 90 degrees to the prescribed (T) direction of crack propagation. Thus, the crack tended to run parallel to the L direction rather than in the T direction in this LT type specimen. Once fast fracture finally occurred however, the macroscopic crack path turned and resumed the designed T direction. This unusual behavior was first thought to be due to anisotropy in the heat of steel possibly alloy banding, inclusion clustering (stringers), or embrittlement of prior austenite grain boundaries by titanium carbide networks formed during hot working.³⁹ No evidence for any of these possibilities could be found in the program heat of 300 maraging steel.

Transmission replica and scanning electron microscopy of fatigue pre-crack fracture regions on the broken K_{Ic} halves revealed that fracture occurred by a mixture of transgranular and intergranular modes. The stress intensity factor range (ΔK) in fatigue for a given compact tension specimen is a function of the specimen thickness, load range, and crack length. The in-house system limitation of 900 kg (2000 lb) has resulted in a de-

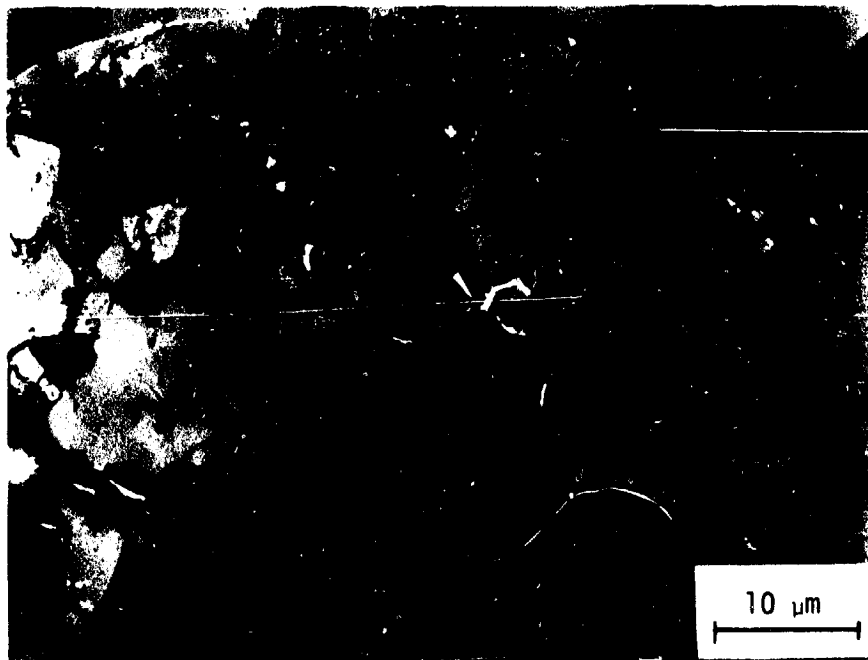
crease in ΔK from about $23 \text{ MN/m}^{3/2}$ ($21 \text{ ksi}\sqrt{\text{in}}$) to $15 \text{ MN/m}^{3/2}$ ($14 \text{ ksi}\sqrt{\text{in}}$) in going from the 1.88 cm (0.75 inch) to the 2.54 (1.0 inch) thick specimen when compared at similar crack length conditions. The 2.54 cm (1.0 inch) thick specimen apparently had more intergranular fatigue than did the smaller specimen. Figure 12 shows examples of TEM replica fractographs of typical transgranular and intergranular fatigue fracture from the fatigue precrack in the 1.88 cm (0.75 inch) and 2.54 (1.0 inch) thick compact tension specimens, respectively. Pelloux and co-workers⁵⁰ have found that the fatigue crack growth rate of annealed and aged 300 maraging steel at low ΔK was significantly lower for specimens tested in dry argon than for specimens tested in air. They⁵⁰ attribute the effect of environment on crack growth rate to a simultaneous presence of oxygen and water vapor. At high ΔK values the crack is advanced before the corrosive effect of the environment can assist in the crack propagation. When the environment has time enough to influence the freshly cracked material, the result is that the crack takes a preferential path along grain boundaries. Thus at low ΔK values, the crack can jump ahead along entire grain surfaces and the crack growth rate is higher than if cracking is confined to normal transgranular crack advance. Because the fatigue precrack in toughness specimens is intergranular, the crack front is effectively following grain boundaries out of a single plane and the result is a branched crack tip. Apparently a varied amount of intergranular crack front exists in specimens given similar aging and precracking. This result could be due to any number of variables, including slight crack length differences and material inhomogeneities. Once precracked, the branched crack tip will delay the fast fracture event to a greater or lesser degree depending upon the resistance to the onset of fast fracture (K_Q), the strain rate of the

K_{Ic} test, the amount of intergranular fracture, and specimen size (degree of plane-strain constraint). In Charpy impact and tensile fractures of an 18 Ni, 350 grade maraging steel, Rack and Kalish⁵¹ have seen intergranular cracks parallel to the tensile loading direction resulting from a strain rate effect. As in their material the effect of the cracks parallel to the tensile direction in this study is to delay the onset of fast fracture. These cracks may be a manifestation of falsely increased ductility or toughness. As the load is applied and the crack is locally deflected into a plane parallel to the major stress axis, it may be effectively blunted and an increase in stress will then be required to re-initiate another crack normal to the tensile axis before fast fracture and failure can be complete. It is important to note that the transverse grain boundary cracks were produced only in fatigue and once they have effectively served to re-channel the main crack front, the crack propagation occurs totally by the usual dimpled rupture process. Although a small fraction of the fatigue crack in the 1.88 cm (0.75 inch) thick high strength specimens was intergranular, the result of relatively low resistance of the material at these strength levels to fast fracture (low toughness) was for the crack to ignore the available transverse paths and fail rapidly. Because of the possible variability in the reaction of the crack tip to the transverse precracked grain boundaries, there is a scatter in the invalid K_Q results which would be difficult if not impossible to explain. The scatter is also due in part to variations in specimen size and fatigue crack length.

The results of six invalid toughness tests including the K_Q , K_{max} (measured from maximum load to break the specimen), the ratio P_{max}/P_5 , and the fatigue stress intensity range at the final fatigue crack length are



Transgranular fatigue in a 0.75-inch thick K_{Ic} specimen



Intergranular fatigue in a 1.0-inch thick K_{Ic} specimen

Figure 12 TEM replica fractographs of typical transgranular and intergranular fatigue fracture in the 18 Ni, 300 grade maraging steel.

listed in Table IV. Note that based upon the thickness criterion of the standard,⁴³ given earlier, the strength of the material produced by a 3 hour, 399°C (750°F) age, and the 2.54 cm (1.0 inch) thickness; the maximum measurable K_Q which will be a valid K_{IC} is approximately $143 \text{ MN/m}^{3/2}$ ($130 \text{ ksi}\sqrt{\text{in}}$). Included in these data are the results of two specimens which were fatigue precracked at slightly higher ΔK values at Westinghouse Research and Development.⁵² Specimens listed in Table IV were all fatigued in room temperature laboratory air. Relative humidity was not measured. Except for one specimen fatigued at 50 Hz the others, as noted previously, were fatigued at 30 Hz. Other than to note the scatter, the only other observation which might be made is that the increase in ΔK from $26 \text{ MN/m}^{3/2}$ ($24 \text{ ksi}\sqrt{\text{in}}$) to $34 \text{ MN/m}^{3/2}$ ($31 \text{ ksi}\sqrt{\text{in}}$) has resulted in a decrease in the measured K_Q . K_{max} has also decreased considerably probably due to less intergranular crack-front and hence less crack rechanneling. Although at a ΔK of $34 \text{ Mn/m}^{3/2}$ ($31 \text{ ksi}\sqrt{\text{in}}$) the intergranular problem still exists, SEM fractography has indicated a slight decrease in the amount of intergranular fatigue. By increasing ΔK significantly more, fatigue in air for this material will revert to a transgranular mode. This will be illustrated shortly. Toughness specimens were not precracked at ΔK levels above $34 \text{ MN/m}^{3/2}$ ($31 \text{ ksi}\sqrt{\text{in}}$) due to the rapid degradation of the fixture for holding the specimen in fatigue.⁵²

Because of the geometric considerations of the tapered design of the Chevron notch fatigue crack starter, when the crack is just starting, ΔK is very large. As the fatigue crack lengthens under fixed load conditions the ΔK decreases until the crack length is just beyond the machine notch. Within a single specimen the qualitative effect of ΔK on mode of fatigue cracking can be monitored. Shown in Figure 13 are SEM fractographs of the

TABLE IV

FATIGUE AND TOUGHNESS DATA FOR THE 18 Ni, 300 GRADE MARAGING STEEL
 AGED FOR 3 HOURS AT 399°C (750°F)

Compact Tension K _{1c} Specimen Thickness cm. (in.)	$\Delta K_{fatigue, a}$ (ksi/ $\sqrt{in.}$) (a, b)	K _Q (ksi/ $\sqrt{in.}$) (a)	K _{max} (ksi/ $\sqrt{in.}$) (a)	P_{max}/P_5
1.88 (0.75)	20.4	85.2	187.4	2.20
1.88 (0.75)	20.2	99.5	186.1	1.87
2.54 (1.0)	13.7	95.8	212.7	2.22
2.54 (1.0)	13.5	136.5	230.7	1.69
2.54 (1.0)	24.2 (c)	217.3	239.1	1.12
2.54 (1.0)	31.0	149.5	183.8	1.23

(a) $1 \text{ ksi}/\sqrt{in.} = 1.1 \text{ MN}/m^{3/2}$

(b) $\Delta K_{fatigue, a}$ = the range in stress intensity factor at final fatigue crack length a

(c) Fatigued at 50 Hz, all others at 30 Hz

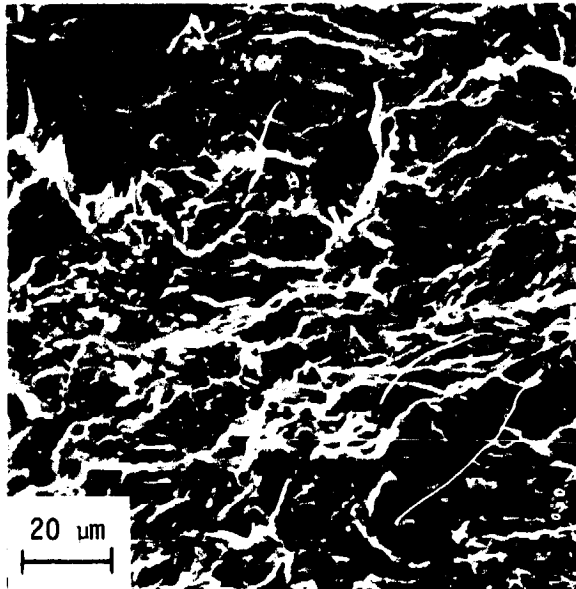


Figure 13a ΔK_1 , near Chevron starter

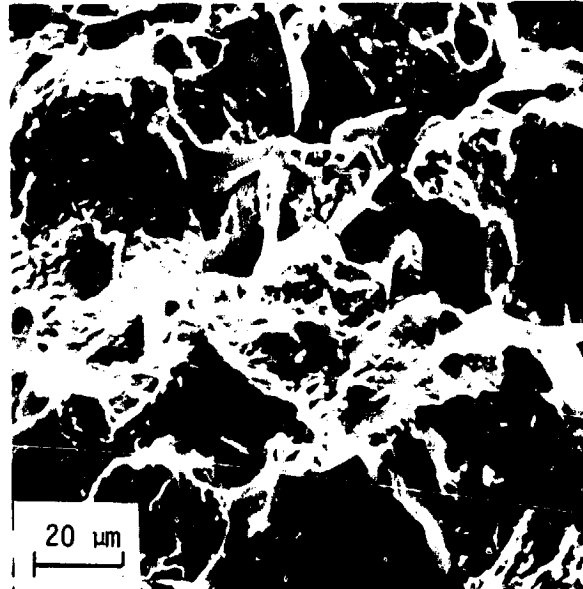


Figure 13b ΔK_2 , further into fatigue region

$\Delta K_1 > \Delta K_2 > \Delta K_3$

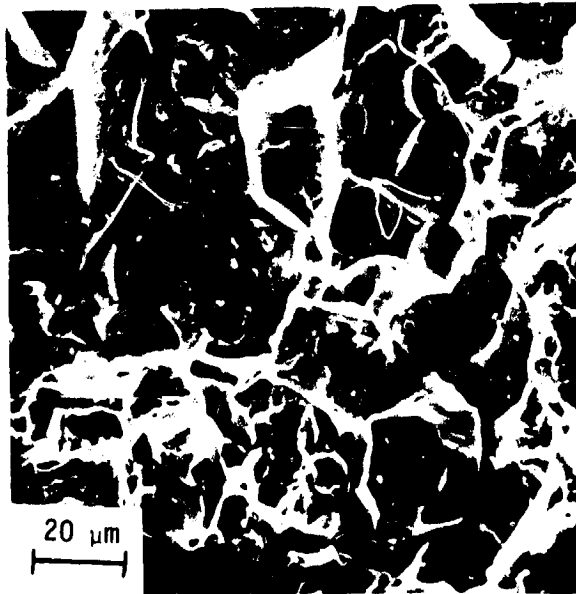


Figure 13c ΔK_3 near end of fatigue crack front

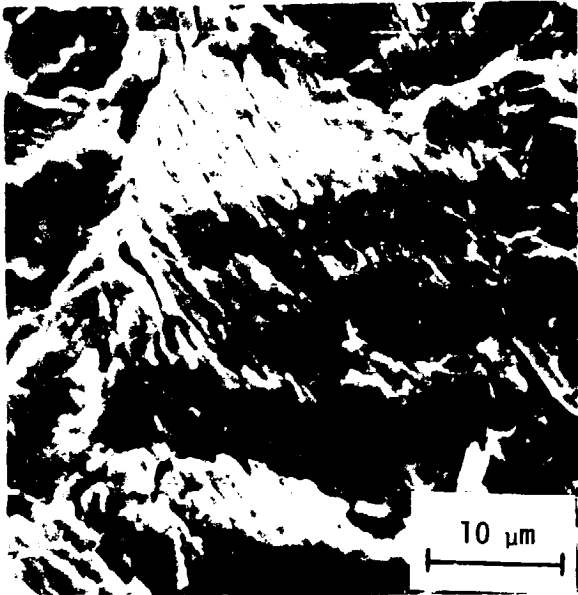
Figure 13 Effect of decreasing ΔK in the Chevron notch of a 1.0-inch thick compact tension K_{IC} specimen. SEM fractographs

fatigue fracture in a 2.54 cm (1.0 inch) thick compact tension specimen fatigued in air. When the crack length is very short and ΔK is large (Figure 13a), the crack propagates by a transgranular mode. At an intermediate crack length and much lower ΔK (Figure 13b), the fracture occurs by a mixed mode. In Figure 13c at the final precrack length when the crack is about 150 mils beyond the machine notch, the ΔK is increasing as the crack lengthens but the mode of fatigue crack advance is still intergranular. In this specimen the fatigue crack front was branched since the fracture is totally intergranular with transverse grain boundaries separated. The result was an invalid test.

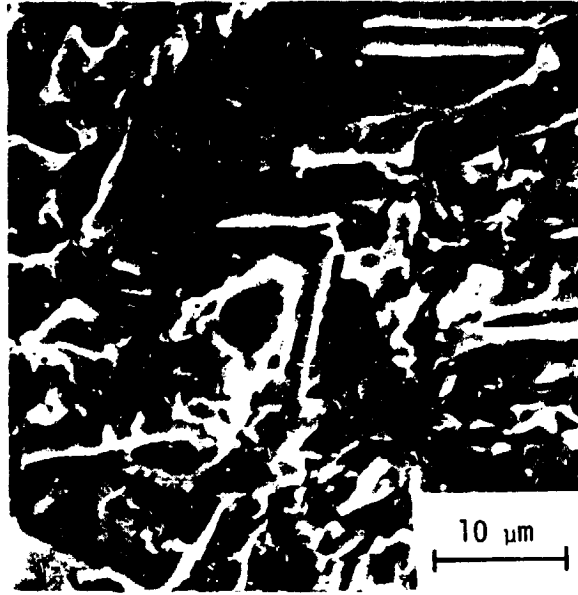
The purpose of this study is to examine the effect of strength and microstructure on toughness. To extend the measurable range in toughness the intergranular fatigue precracking problem must be eliminated. The effect of environment (moist air) on the mode of fatigue fracture in 300 grade maraging steel can be suppressed by increasing ΔK beyond some critical value or by replacing the environment with one that is inert. In a study to control ΔK in air, standard size sharp notched Charpy specimens aged for 3 hours at 399°C (750°F) were precracked as a function of ΔK . At a ΔK of 44 $\text{MN}/\text{m}^{3/2}$ (40 $\text{ksi}\sqrt{\text{in}}$) the fracture clearly has the frequently observed transgranular, striated appearance shown in Figure 14. Decreased by a factor of 5, at a ΔK of 9 $\text{MN}/\text{m}^{3/2}$ (8 $\text{ksi}\sqrt{\text{in}}$) the fracture is totally intergranular. At an intermediate ΔK the fracture is transgranular but clearly not striated. In air, the results of all testing suggest that fatigue must be performed at a ΔK of at least 39 to 44 $\text{MN}/\text{m}^{3/2}$ (35 to 40 $\text{ksi}\sqrt{\text{in}}$) to sufficiently reduce the effect of environment.

As an alternative to increased ΔK , dry argon was used as the atmosphere for fatiguing a Charpy. The Charpy specimen and entire holding

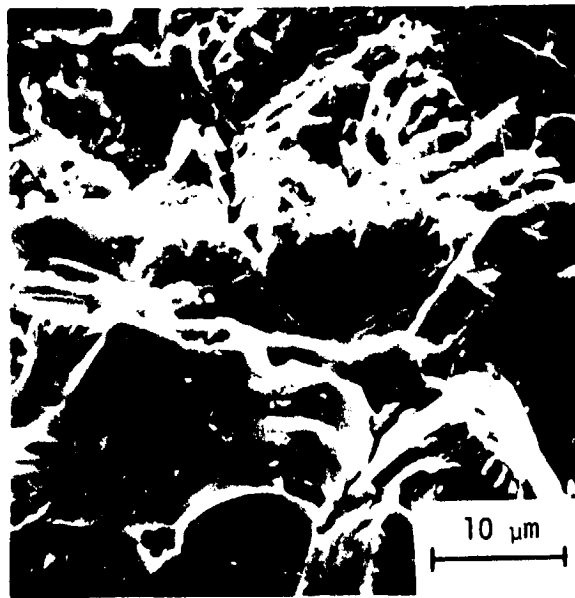
fixture were enclosed in a plastic bag. Argon was passed through a drying tower and a titanium gettering furnace operated at about 750°C (1382°F) to eliminate moisture and residual oxygen. Fatigue cracking was performed at a low ΔK of about $11 \text{ MN}/\pi^{3/2}$ ($10 \text{ ksi}/\sqrt{\text{in}}$) to make certain the effects seen would be due to the dry argon atmosphere. The expected elimination of intergranular fatigue by the presence of argon was confirmed in Figure 15. The Charpy specimens fatigued to failure in air and argon broke in about 130,000 and 850,000 cycles respectively which confirms the decrease in crack growth rate in argon observed by Pelloux and co-workers.⁵⁰ A protective argon atmosphere is being considered for precracking of fracture toughness specimens.



$\Delta K = 40 \text{ ksi}\sqrt{\text{in.}}$



$\Delta K = 20 \text{ ksi}\sqrt{\text{in.}}$



$\Delta K = 8 \text{ ksi}\sqrt{\text{in.}}$

Figure 14 SEM fractographs of fatigue in air of Charpy specimens precracked at controlled ΔK levels.

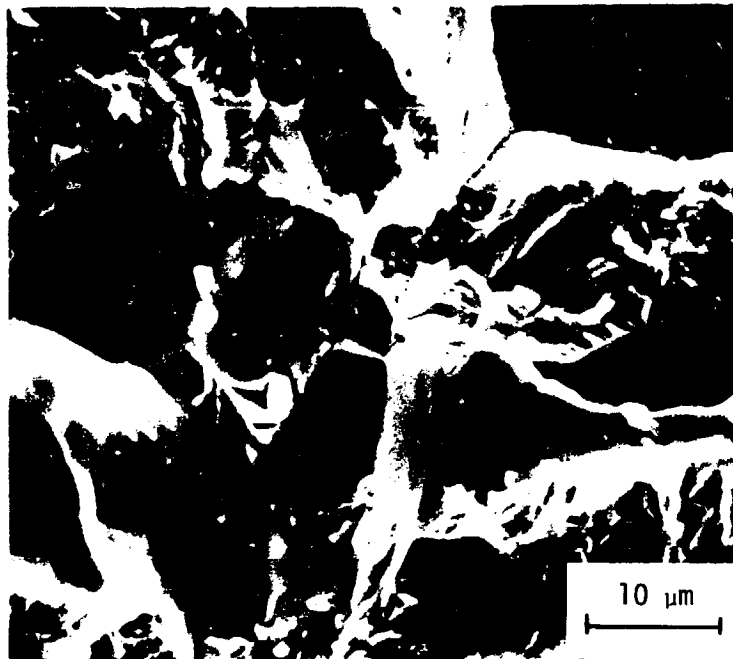


Figure 15a Room temperature air

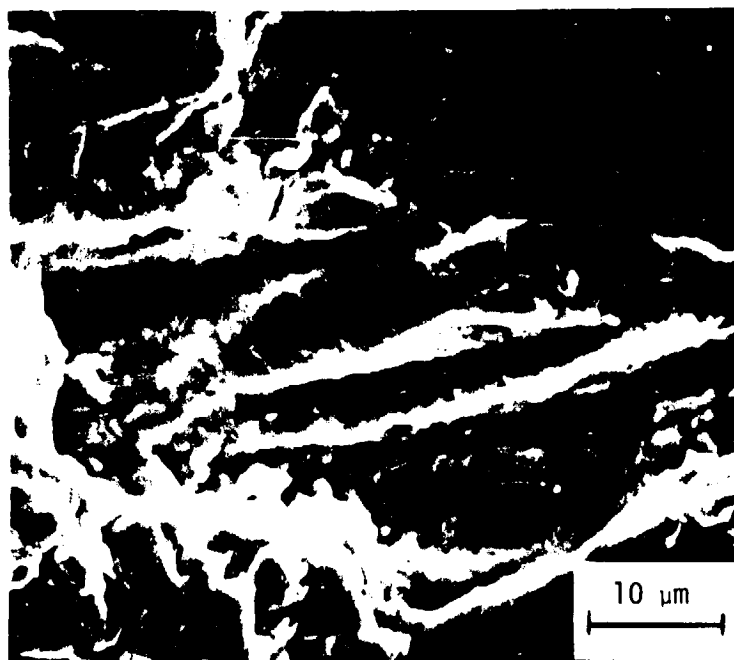


Figure 15b Room temperature dry argon

Figure 15 SEM fractographs of intergranular fatigue in air, figure 15a, and transgranular fatigue in dry argon, figure 15b. $\Delta K = 10.5 \text{ ksi}\sqrt{\text{in.}}$

FRACTOGRAPHY

A fractographic study was carried out on the variously aged 18 Ni, 300 grade maraging steel to characterize the fracture surfaces. The fracture surfaces from compact tension specimens (K_{IC} specimens) and smooth, round tensile bars were examined for each of the strength levels listed in Table II. The K_{IC} fractures observed included only those for which valid data currently exists. The central regions of all the smooth tensile fractures were viewed with the exception of the solution treated and the 100 hour, 427°C (800°F) aged specimens. All specimens which result from future work, including those not considered thus far, will be thoroughly examined in the next phase of this study. Limited fatigue precracked Charpy fracture surfaces were examined since plane-strain fracture toughness is, by design, the choice for measurement of toughness. Examination of the available valid 1.88 cm (0.75 inch) thick compact tension specimen fracture surfaces in a stereo microscope at low magnification showed them to be rough and fibrous in appearance. The smooth, round tensile bars at all strength levels considered exhibited a cup and cone type fracture. With decreasing strength level the size of the shear lips increased and the area of central flat fracture region decreased, both indicative of increasing ductility. The central regions of all the tensile bars were rough and fibrous in appearance at low magnification. The topography of the low strength tensile fracture was extremely rugged by comparison to the relative flat surface of the fully strengthened tensile. In general, the fracture surface roughness decreased with increasing strength.

Two stage, cellulosic acetate-platinum shadowed carbon replicas were

taken from the areas of fast fracture initiation on the K_{IC} fracture surfaces and from the central regions of normal rupture on the smooth tensile fracture surfaces for each available condition. These replicas were examined using an electron microscope. In all cases stereo pairs were taken of each area viewed. By suitably tilting the specimen by 6 degrees from its initial orientation, the pair of fractographs produced can be viewed in a stereo viewer which results in a fracture surface that appears three-dimensional. With these techniques it was found where comparisons could be made that the features on the fracture surfaces were qualitatively the same for both the tensile and K_{IC} fracture tests for any given strength level. The fracture mode at all strength levels observed was dimpled rupture. Dimpled rupture is the mode of fracture whereby microscopic voids nucleate at second-phase particles, then grow and coalesce to cause final rupture. This fracture mode is also called microvoid coalescence or plastic fracture. This mode of fracture is termed dimpled rupture since both halves of the fracture surface are covered by depressions, or dimples, which have formed due to void formation at a second-phase particle, void growth, and void coalescence.

To remain realistic about the strength range for which valid K_{IC} fractures can be made available, the smooth tensile fractures will be examined here for only the 3 hour, 344°C (650°F) aging temperature and above. Examples of the types of features observed at each strength level will be noted. Where possible, one example will be from a smooth tensile fracture and one from a valid K_{IC} fracture. In all cases, except where noted, there will be two examples for each strength level on a given figure. The qualitative similarity between the K_{IC} and tensile fractures should become apparent for the selected comparisons available. The plan

has been to provide an initial characterization of the fracture in the 18 Ni, 300 maraging steel as a function of strength. Ultimately in this program, techniques similar to those used in quantitative optical metallography will be used on the final set of tensile and K_{IC} fractures to measure the sizes and areal fractions of various fractographic features. The fractographic behavior as a function of strength will be compared to direct observations of the microstructure from variously strained and sectioned tensile specimens. The progress made thus far on characterizing the fracture surfaces will be discussed as the fractographs for each strength level are presented. Tensile- K_{IC} fracture surface comparisons are made only for the 3 hour aging treatments at 427°C (800°F), 482°C (900°F), and 538°C (1000°F).

With increasing strength and/or overaging, the dimples covering the fracture surfaces decrease in size and it appears that a larger fraction of the size distribution of second-phase particles have participated in void formation. As strength is increased the critical size impurity inclusions for void initiation apparently decreases since evidence of smaller particles is present on higher strength fractographs. Since strengthening precipitates grow with extent of aging, there is some evidence that these second-phase particles may be active sites for void coalescence if the strength and/or overaging combination is correct. The 3 hour, 344°C (650°F) aged room temperature tensile fracture surfaces (Figure 16a and b) are covered almost completely by equiaxed dimples approximately 10-20 μm in diameter. There are also a few finer dimples which are a few microns in size. The occurrence of these smaller dimples marked "Y" are, however, infrequent in this condition. The large dimples are marked "X" on the fractographs. Although Ti(C,N) inclusion impressions are not clearly

evident here, there is evidence of void initiation sites marked by arrows. These may be the elongated Ti_2S particles.

With increasing strength, examples of the fracture surfaces of smooth tensile specimens aged for 3 hours at $371^{\circ}C$ ($700^{\circ}F$) are shown in Figure 17. There now appears to be a greater number of dimples within an area equal to the fractographs of Figure 16. Very few dimples are as large as $15\ \mu m$ in diameter. The majority of the fracture surface is now covered by dimples from $5-10\ \mu m$ in size. Small inclusions evidently of the $Ti(C,N)$ type occupy sites marked "X" in Figure 17a. Indicated by an arrow in Figure 17a is the impression of an inclusion approximately $5\ \mu m$ long and $2\ \mu m$ wide which may have failed by interface separation as revealed by the replicating tape which has surrounded the particle. In Figure 17b are fragments of inclusions which have broken up and have been extracted from the fracture surface. The fragments which are too thick to transmit the electron beam are marked as "Y."

An increase in strength of about $345\ MN/m^2$ (50 ksi) over the $344^{\circ}C$ ($650^{\circ}F$) condition, the $399^{\circ}C$ ($750^{\circ}F$) age has resulted in dimples that appear less equiaxed and between $5-10\ \mu m$ in size. These tensile fractographs shown in Figure 18 show areas which appear as large dimples which contain many smaller dimple markings. At "X" in Figure 18a are many fragments of inclusions. Arrows mark void nucleation sites lying at the bottoms of small but very deep equiaxed dimples. The abrupt level changes and heavily marked dimples of Figure 18b are best seen by stereo viewing. It was necessary to observe several fractographs from the $399^{\circ}C$ ($750^{\circ}F$) aged material in addition to those of Figure 18 before the trend for decreasing dimple size with increasing strength could be confirmed. Until quantitative fractography is performed to characterize the fracture sur-



Figure 16a Smooth tensile

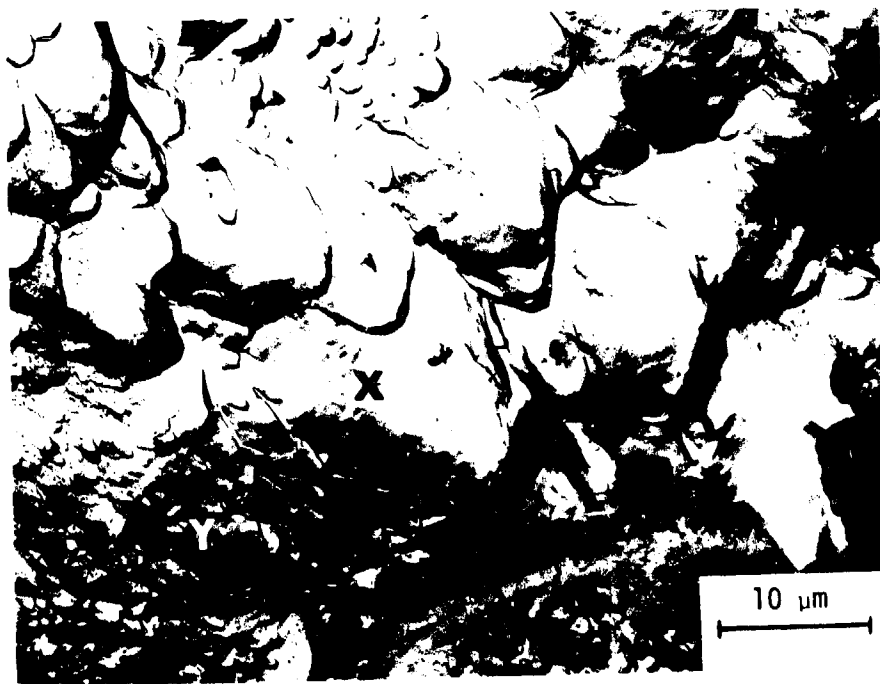


Figure 16b Smooth tensile

Figure 16 TEM fractographs of smooth tensile fractures (a and b) of the 18 Ni, 300 grade maraging steel aged for 3 hours at 344°C (650°F). (Regions of large dimples are marked "X" and small dimples are marked "Y." Arrows point to void initiation sites.)



Figure 17a Smooth tensile

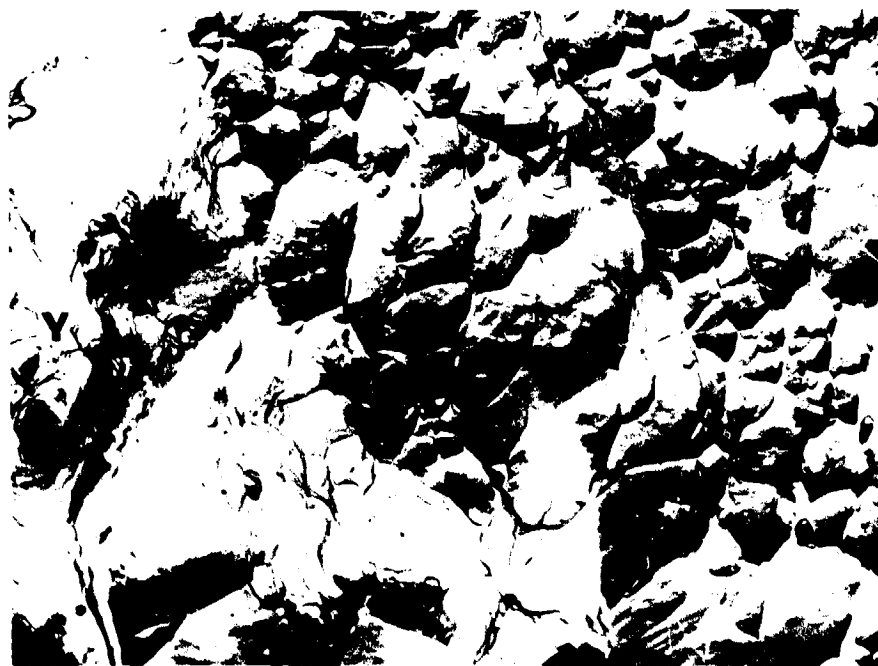


Figure 17b Smooth tensile

Figure 17 TEM fractographs from tensile fractures (a and b) of the 18 Ni, 300 grade maraging steel aged for 3 hours at 371°C (700°F). (A small dimple region and an initiation site are marked by "X" and an arrow respectively in figure 17a. Extracted fragments of inclusions are shown in figure 17b marked by "Y.")



Figure 18a Smooth tensile

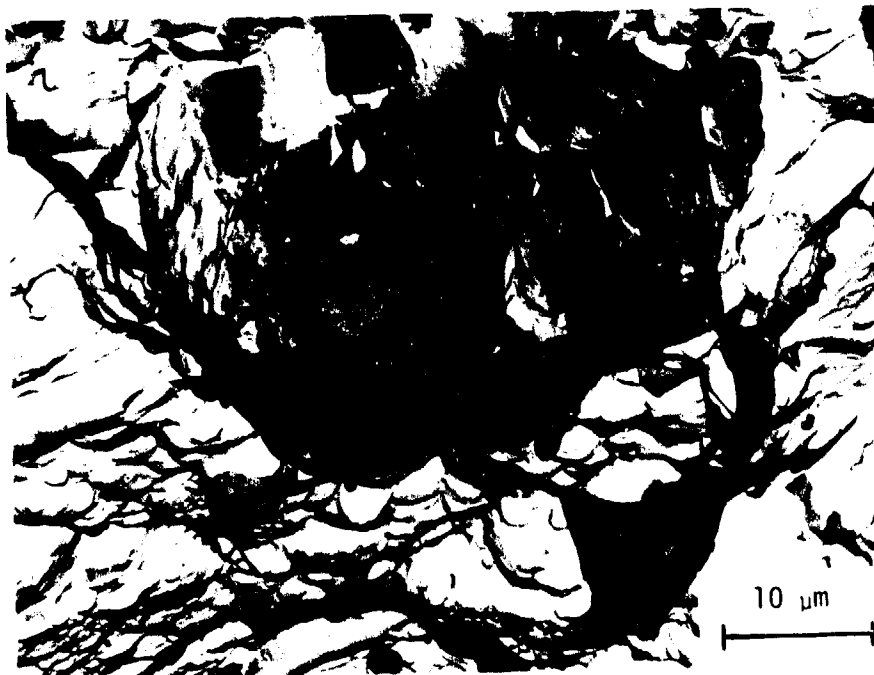


Figure 18b Smooth tensile

Figure 18 TEM fractographs from tensile fractures (a and b) of the 18 Ni, 300 grade maraging steel aged for 3 hours at 399°C (750°F). (At "X" in figure 18a are many fragments of inclusions. Arrows mark void initiation sites.)

faces, these qualitative observations are clearly subject to revision.

An increment in strength of about 173 MN/m^2 (25 ksi) has resulted in an activation of particles that are often less than $1 \mu\text{m}$ in diameter. In turn the fractographs are complex regions of dimples rarely $5\text{-}7 \mu\text{m}$ in size but rather dimples that are 1 or $2 \mu\text{m}$ in diameter. The similarity of features in the 427°C (800°F), 3 hour aged tensile (Figure 19a) and K_{IC} (Figure 19b) fracture is evident. Associated with many of the fine dimples of Figure 19a are submicron initiation sites at the bottoms of these dimples (marked with an arrow). $\text{Ti}(\text{C},\text{N})$ inclusions a few microns in size are marked "X" in Figure 19b. These fine dimples often appear in colony-like patches as marked "C" in Figure 19b.

At approximately 1863 MN/m^2 (270 ksi), the tensile and K_{IC} fractures from material aged for 3 hours at 482°C (900°F) contain dimples that are typically less than from 3 to $5 \mu\text{m}$ and frequently of submicron dimensions. Many small inclusions appear to have been extracted and are marked by arrows on the tensile fracture shown in Figure 20a. The submicron size dimples appear to frequently surround larger dimples and are oriented on ledges. These ledges of very fine markings are shown in the tensile fracture (Figure 20a) and particularly in the K_{IC} fracture (Figure 20b) marked "L." Apparently the critical size inclusion that can be an active void initiation site decreases as strength increases. There is an extensive range in particle sizes which can initiate voids at a strength level such as 1863 MN/m^2 (270 ksi). With increasing strength, the number of void nucleation sites apparently increases as evidenced by the series of fractographs shown in Figures 16 through 22. That is, with increased frequency of void initiation, the fractographs from less tough material are covered with a larger number of small dimples. It is also apparent from Figures 19 through 22

that the dimples are frequently 1 μm or less in size and hence the decrease in dimple size with decreasing toughness over this range is not obvious from these few fractographs. This relatively small change in dimple size over this range in strength may be attributed in part to the less rapid decrease in toughness in this high strength range shown in Figures 9 and 10. There is, however, an increased frequency of formation of ledges of submicron dimples with decreasing K_{IC} .

As the strength increases due to growth of strengthening precipitates these second-phase particles may at some critical combination of strength and particle size become active void initiation sites. In a similar manner, Cox and Low⁴ have shown that the strengthening precipitates may aid in the void coalescence process. The ledges of submicron dimples in Figure 20b may be the fractographic appearance of such a process. Speculation for the role of precipitates in void coalescence will be examined at incremental stages in the void initiation, growth, and coalescence process by a sectioned tensile technique.

The next condition in order of decreasing ductility is the overaging treatment for 3 hours at 538°C (1000°F). As compared to the 3 hour 482°C (900°F) aging treatment there is a loss in strength of about 173 MN/m² (25 ksi). The overaged tensile (Figure 21a) and K_{IC} (Figure 21b) fractures are similar with the largest dimples above 5 μm . Again, unlike at low strength levels, the dimples are not very equiaxed. The areal fraction of these fracture surfaces covered with submicron size dimples is apparently quite high. These ledge-like regions are marked in Figures 21a and 21b by "L." There are a number of extracted inclusion fragments marked by arrows and the impression of a Ti(C,N) indicated by a small "c" in the K_{IC} fractograph of Figure 21b.

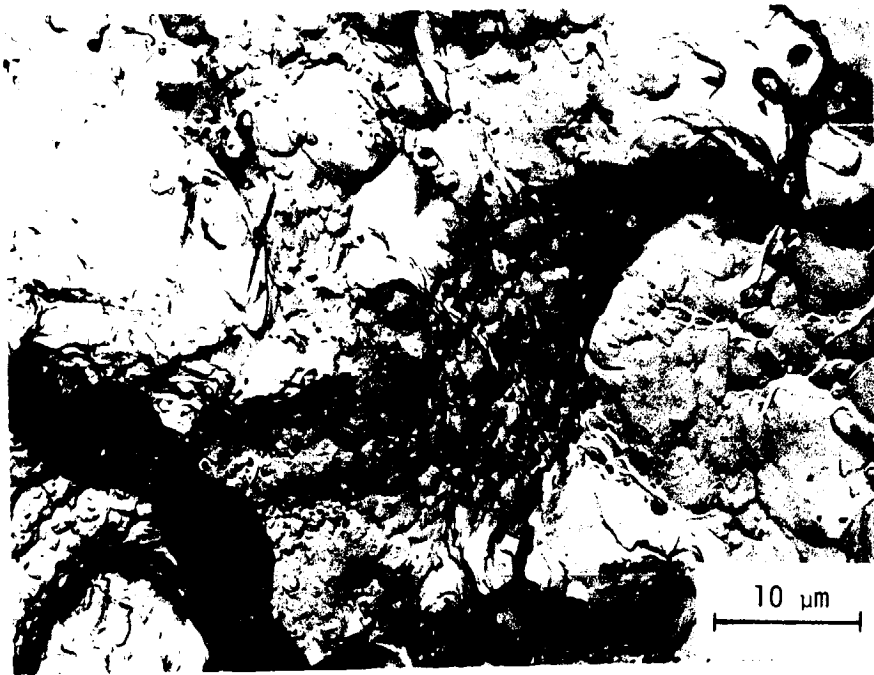


Figure 19a Smooth tensile

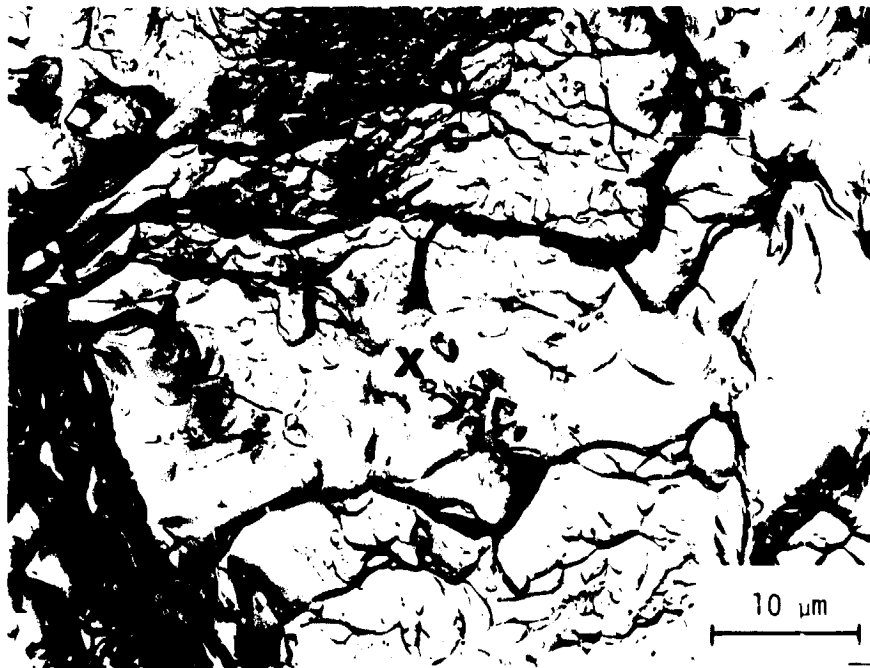


Figure 19b K_{IC}

Figure 19 TEM fractographs from (a) tensile and (b) K_{IC} fractures of the 18 Ni, 300 grade maraging steel aged for 3 hours at 427°C (800°F). (Arrow points to void initiation sites in figure 19a and initiation sites are marked "X" in figure 19b. Colony-like patches are marked "C" in figure 19b)

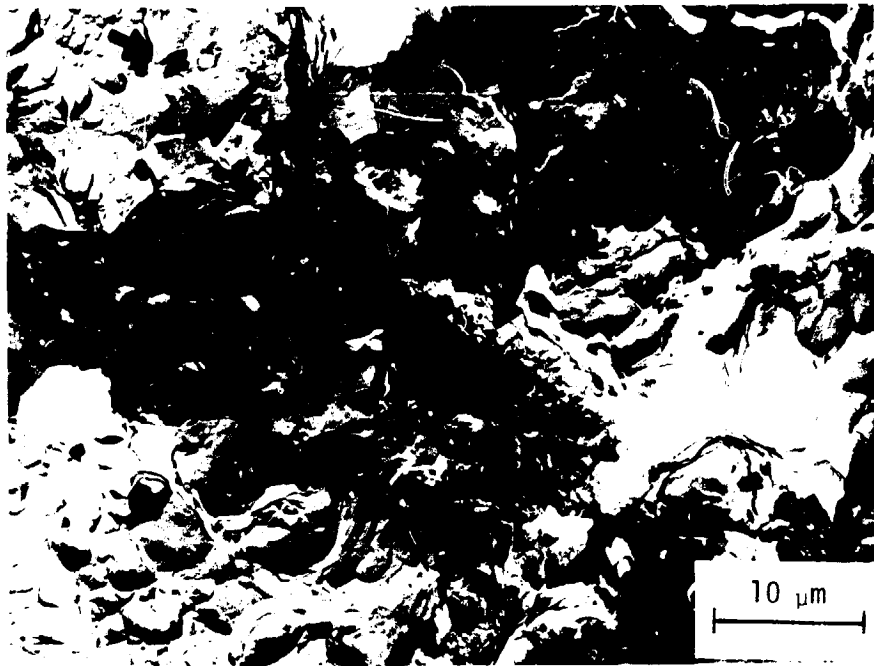


Figure 20a Smooth tensile

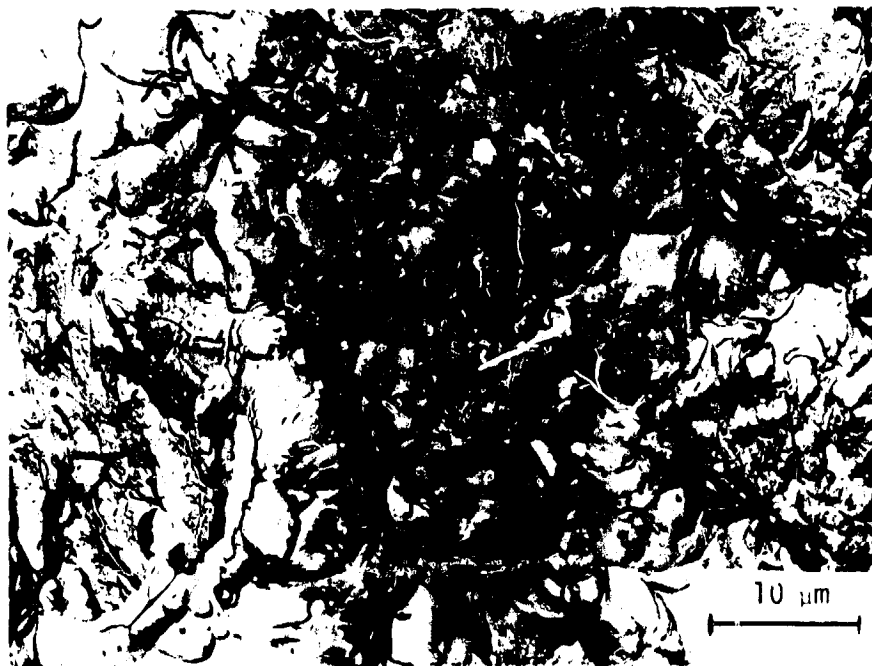


Figure 20b K_{IC}

Figure 20 TEM fractographs from (a) tensile and (b) K_{IC} fractures of the 18 Ni, 300 grade maraging steel aged for 3 hours at 482°C (900°F). (Ledges of fine dimples are marked 'L' in figure 20b.)

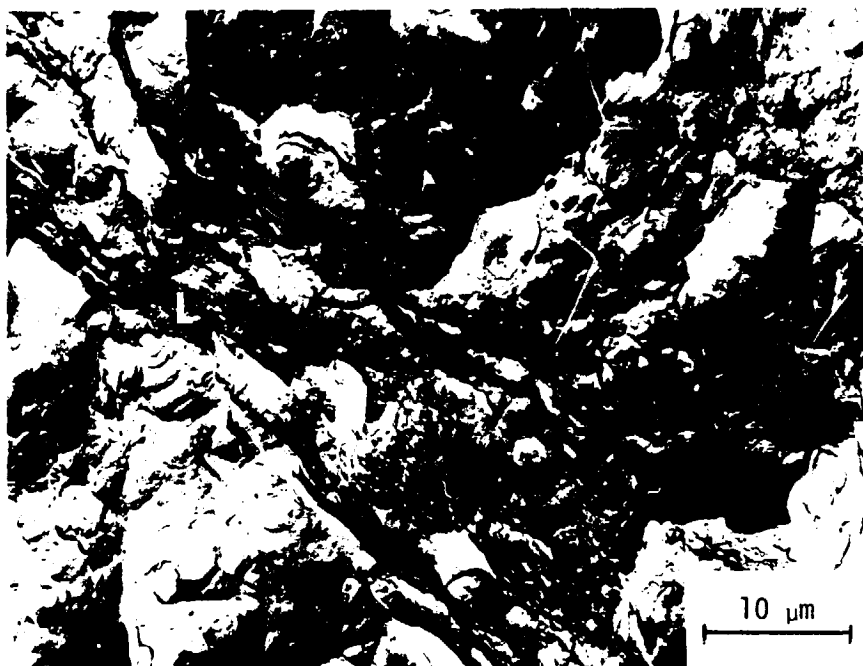


Figure 21a Smooth tensile

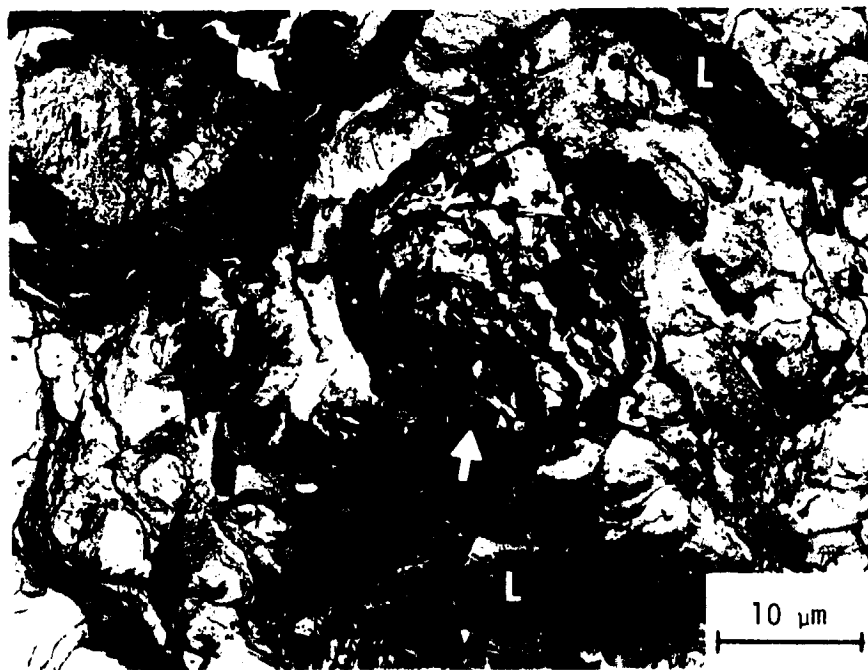


Figure 21b K_{IC}

Figure 21 TEM fractographs from (a) tensile and (b) K_{IC} fractures of the 18 Ni, 300 grade maraging steel aged for 3 hours at 538°C (1000°F). Ledge-like regions are marked by "L." Inclusion fragments are marked by arrows and the impression of a Ti(C,N) is marked by a small "c" in figure 21b.)

The fully aged condition produced by a 100 hour aging treatment at 427°C (800°F) resulted in the lowest fracture strain and K_{IC} of all the strength levels considered. As tensile fractures in this condition have not yet been replicated, typical fracture surfaces of K_{IC} specimens are shown in Figure 22. The extracted particles and their impressions in the replica shown in Figure 22a are similar in shape to the Ti_2S inclusions seen in polished sections. The regions marked "L" are very steeply inclined ledges of submicron size dimples. The dimples in this condition are very angular, stepped, and non-equiaxed. Figure 22b particularly shows these angular features. The sharp level changes are more dramatically illustrated with stereo pairs. These ledges of submicron dimples appear to be in a stepped or lamellar arrangement. Submicron size dimples also cover sharply inclined regions in the fractures of lower strength material (Figures 20 and 21) but to a lesser degree than in the fully strengthened material. The areal fraction of stepped regions covered with submicron size dimples is clearly quite high. A more exact correlation of the lamellar steps in these fractographs to the low toughness in this condition other than that dimples are extremely small is unclear at this time. An example of a higher magnification fractograph taken of a ledge area similar to those in Figure 22 is shown in Figure 23. The fine markings on these stepped regions are very fine dimples. The arrows in Figure 23 point to evidence of depressions in these dimples which may be related to strengthening precipitates since they are much less than 0.1 μm .

A complete characterization and relation of microstructure to fracture mechanism as a function of strength in the 18 Ni, 300 grade maraging steel will require further examination of stereo pairs, quantitative fractography, and a direct observation of the stages of fracture via sectioned tensile specimens.

DISCUSSION OF RESULTS AND FUTURE WORK

It has been demonstrated above and in work which has been previously reported¹ that there is a significant inverse relationship between strength and toughness in the 18 Ni, 300 grade maraging steel. The observed fractographic trend for decreasing dimple size with increasing strength and/or overaging suggests that the deformation and microstructural characteristics of the material determine the relative importance of the initiation, growth, and coalescence stages of fracture. While fractography is a key technique for studying the morphology of microstructure which contributes to fracture, the conclusions drawn are limited to observations made after the event of fracture. To relate the fracture mechanism as a function of strength to the microstructure, a means of directly observing the microstructure as the dimpled rupture process progresses is necessary. The fracture mechanism will be studied by several sectioned tensile samples which have been strained short of fracture for each strength level. The sectioned tensile technique and the sectioning results to date will be presented. Based upon evidence to date, a mechanism for fracture as a function of strength in 18 Ni, 300 grade maraging steel will be discussed along with further work which is required to clarify the inverse relationship between strength and toughness. The model proposed is the best estimate of how the changing strength and microstructure affect the toughness. Although speculative, the model is important as an aid to designing critical experiments which can reinforce or refute the present mechanism proposed.



Figure 22a K_{Ic}

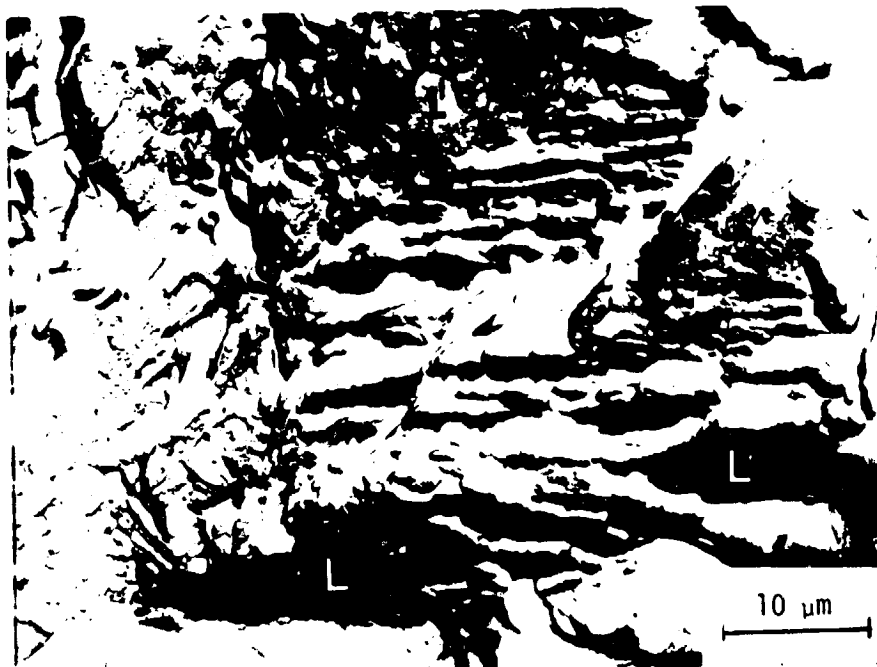


Figure 22b K_{Ic}

Figure 22 TEM fractographs from K_{Ic} fractures (a and b) of the 18 Ni, 300 grade maraging steel aged for 100 hours at 427°C (800°F). (Regions marked "L" are steeply inclined ledges of submicron size dimples.)



K_{Ic}

Figure 23 TEM fractograph from a K_{Ic} fracture of the 18 Ni, 300 grade maraging steel aged for 100 hours at 427°C (800°F). This is a typical high magnification fractograph of a ledge area similar to those shown in figure 22. (Impressions of submicron initiation sites are indicated by arrows.)

A. Sectioned Tensiles

The success of the sectioned tensile technique rests primarily on establishing that the plane-strain fracture toughness and smooth round tensile fracture mechanisms are similar. With K_{IC} tensile fractographic similarity confirmed, tensile specimens aged for 3 hours at 427°C (800°F), 482°C (900°F), and 538°C (1000°F) were variously strained short of fracture and sectioned to the midplane in each specimen. The first step after straining is grinding to within 3 mils of the specimen midplane. Grinding was done to reveal the plane normal to the thickness direction in the plate, that is, the plane defined by the L and T directions. Specimens were then cut from the tensile barrel, mounted in Bakelite and ground through 320, 400, and 600 grit silicon carbide papers using automated metallographic grinding equipment. The specimens were then hand polished using 6, 3, and 1 micron diamond paste. Vibratory polishing in a slurry of 0.05 micron alumina powder in distilled water completed the steps. Specimens were viewed in an optical microscope at 500X. A more detailed sectioning study is in progress which includes 10 specimens per aging condition varying from the elastic strain at yielding to as close to fracture as possible without failure. The advanced program includes several strength levels and has not yet been completed.

To date, no quantitative analysis has been performed on the void nucleation, growth, or coalescence stages of fracture. The sequence of events taking place with plastic straining and the role of inclusions in this process are roughly illustrated in Figure 24. In these micrographs the tensile axis is vertical. Shown are optical micrographs of the 1553 MN/m² (225 ksi), 3 hour, 427°C (800°F) aged tensile specimens at three levels of straining. At a plastic strain of 0.150, Figure 24a shows

an elongated Ti_2S inclusion which has several cracks associated with it. There is also a small $Ti(C,N)$ which evidently has not yet cracked. From another specimen of the same strength at a strain of 0.551 (Figure 24b), there appears to be more voided area than at the lower strain of Figure 24a. Because this is only one example, Figure 24b may not be the best example to indicate the extent of void growth at a strain of 0.551. At the final plastic strain of 0.732 that was examined at this strength level, the amount of void growth is clearly shown by Figure 24c. The large void is indicated by a small "v" and open arrows indicate some of the particle fragments attached to the void walls. Also shown by a solid arrow is a possible site of void coalescence between two larger voids. The fracture strain for material of this strength is 0.778.

Figure 25 shows two examples of typical methods of void formation. The plastic strains in these micrographs were not chosen for any particular reason. These micrographs were taken from material aged for 3 hours at $482^{\circ}C$ ($900^{\circ}F$). Figure 25a is an example of void formation by particle cracking. The particle appears by its shape to be a $Ti(C,N)$. Particle failure at least partially by particle-matrix interface separation is indicated by an arrow in Figure 25b. From these limited observations at selected increments of strain, the fracture mechanism as a function of strength cannot be precisely characterized. The sectioned tensile technique is a viable technique for directly observing the events at various stages up to fracture. This method should also provide the means for linking the role of microstructure in the various stages of fracture to the fractographic appearance. The amount of deformation necessary to activate various void nucleation sites and the amounts of void initiation, void growth, and void coalescence as a function of strength level can be de-



Figure 24a $\epsilon = 0.150$



Figure 24b $\epsilon = 0.551$

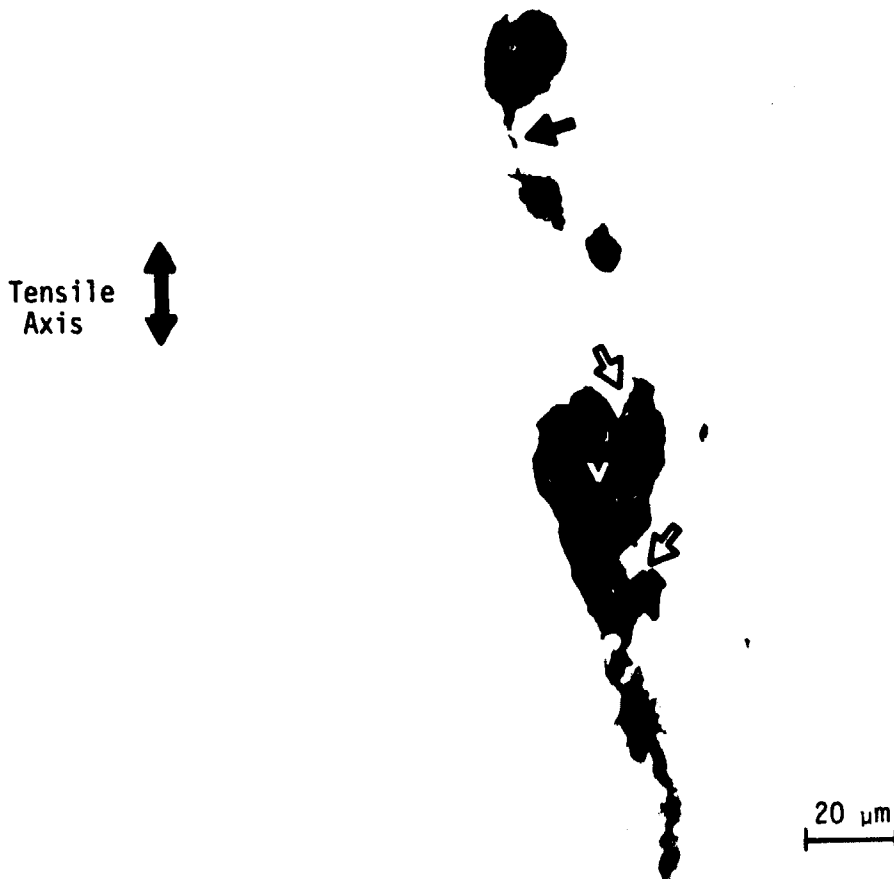


Figure 24c $\epsilon = 0.732$

Figure 24 Void initiation and growth in smooth tensiles aged 3 hrs. at 427°C (800°F). Fracture strain for condition is 0.778. (In fig. 24c large void is marked "v" and open arrows indicate particle fragments. A solid arrow indicates a possible site of void coalescence between two large voids.)



10 μm
┌───┐

Figure 25a Particle cracking, $\epsilon = 0.151$

Tensile
Axis 



10 μm
┌───┐

Figure 25b Particle-matrix interface separation, $\epsilon = 0.322$

Figure 25 Void initiation in tensile specimens aged for 3 hours at 482°C (900°F) and variously strained. Figure 25a shows a Ti(C,N) that has cracked. Particle failure at least partially by particle-matrix interface separation is indicated by an arrow in figure 25b.)

terminated by sectioning. This information cannot be determined from observations made solely from fracture surfaces.

B. Proposed Model

The proposed mechanism for fracture as a function of strength in the 18 Ni, 300 grade maraging steel must include a suitable explanation of several details of the mechanical properties and fractographic appearance observed in this study. First, why with increasing strength and/or overaging does the dimple size decrease? Also, the resulting number of dimples appears to increase. Second, is there a critical size particle for void initiation? If so, which variables are controlling as a function of strength? Third, do strengthening precipitates, which grow with aging (strength level), behave according to a critical size dependence so that at some strength level and size combination they become active void nucleation sites for coalescence of the large inclusion nucleated voids?

The model which will be presented is based on the observations made in this investigation, on various findings in the literature, and that fracture occurs by some combination of void initiation, growth, and coalescence of voids at all levels of strength considered. At this stage in the investigation the mechanism proposed is based upon reproducible evidence as well as a considerable amount of speculation. The exact effect of microstructure and strength on the fracture toughness and fracture mechanism of this material is not well understood and thus the model to be given should be accepted with awareness of these limitations.

The 18 Ni, 300 maraging steel fails by dimpled rupture at all strength levels considered. The model to be presented will deal separately with the three generally recognized stages of fracture: void initiation, void growth, and void coalescence. The initiation step consists of the nuclea-

tion of microvoids at second-phase impurity inclusions in the material. Evidence indicates that this event might occur by inclusion cracking of the titanium carbonitrides and decohesion along the interface between the titanium sulfides and the matrix. The key variables which control void initiation as a function of strength are thought to be the applied stress and the inclusion size (average diameter). Roesch and Henry² have shown evidence for a size effect and have suggested the concept of a critical particle size for cavity nucleation. Cox and Low⁴ have shown that for a fixed strength level the largest inclusions initiate voids at lower strains. When examining material at several strength levels and a fixed value of strain, it is expected from these arguments that there will be more inclusion nucleated voids present in the material having a higher applied stress. For a constant strain the higher applied stress in stronger material is illustrated in the flow curves of Figure 11. Likewise with increasing strength, a critical level of flow stress would be attained at a much earlier stage in the strain or deformation process. The belief is that the entire process of void initiation would be shifted to lower strains in higher strength material. Whether or not the initiation requires plastic strain in addition to the elastic component will be checked at each strength level in further sectioning work. By increasing the strength, the potential void sizes would be reduced due to an increase in the void initiation frequency and less required growth for void linkup.

In a higher strength material a larger fraction of the fixed inclusion population satisfies a critical size criterion at some point in the strain history, the result being a decrease in K_{IC} . As observed in higher strength material the fractographs are covered by small dimples corresponding to the small voids. Conflict exists between experimental findings and theoretical

analyses. Continuum elastic stress analyses^{21,22} indicate that the stress concentration at a particle is independent of its size. Ashby,²⁷ however, has presented a dislocation model of a rigid particle in a slip band where the shear stress component from the slip band is proportional to the particle diameter. This model too would support a size effect since a larger particle will have a larger localized stress concentration associated with it.

As the stresses are increased beyond the level at which void nucleation first occurs, regardless of the strength level, the voids which have initiated at inclusions grow by some mechanism involving plastic flow of the matrix. With continued straining, inclusions of decreasing size could fail while the currently existing voids grow. It is believed that the controlling variable for void growth is the flow stress of the material. The rate of void growth might be expected to decrease as the yield strength increased since there would be more resistance to plastic deformation in the matrix. The analyses of McClintock²⁸ and Rice and Tracey³⁷ for the stress states existing around inclusions, holes, and at the tips of cracks indicate that the rate of void growth increases with increasing strain for both strain-hardening and non-strain-hardening materials and that the existence of a state of triaxial tension should accelerate the rate of void growth. Since the amount of void growth would be related to the spacing between voids, the amount of growth would decrease in higher strength material due to the presence of a larger number of voids per unit volume. Because finite spacing exists between voids, interaction of the stress fields may influence void growth. As the spacing between voids decreases the interaction effects may become more important. It is probable that the interaction will promote coalescence. The reduction in dimple size with

increasing strength is an indication of less void growth. There is very little evidence to date to support any of the trends expected.

Of the three stages of dimpled rupture, void coalescence is the least understood. The variables controlling void coalescence are expected to be the size of second-phase particles (namely the strengthening precipitates), the applied stress, the planarity of slip, and the spacing between inclusion nucleated voids. Cox and Low⁴ have shown that the amount of plastic deformation which may occur before fracture and, also, the fracture toughness, is strongly affected by whether or not voids grow to impingement or the void growth process is interrupted by void sheet formation. Fractographic evidence of submicron dimples on ledges in the 300 grade maraging steel of this study indicates that a void sheet mechanism may be operative at strengthening precipitates in the fully aged and overaged material. A critical combination of precipitate size and applied stress will exist in higher strength material thus causing large void linkup short of impingement. In recent work on high-strength aluminum alloys, Hahn and Rosenfield³⁸ have attributed a substantial loss of fracture toughness with increasing yield strength level to a reduction in the work needed to link the voids in the higher strength alloys. These authors³⁸ connect the loss in toughness with the fine precipitates that form during aging, the loss of strain hardening capacity, and the development of intense shear bands due to more planar slip in higher strength conditions. In the high strength material slip is more planar, precipitates are larger due to the degree of aging, spacing between voids is reduced due to increased frequency of void initiation, and interaction effects are more intense due to reduced intervoid spacing. All these factors increase the prospect for a more rapid coalescence of voids either by impingement or by void sheets with the likelihood

of void sheets enhanced with strength and/or overaging. Because void coalescence occurs so rapidly the event is difficult to stop short of final fracture. Electron beam instrumentation such as TEM and SEM may be required to examine microstructure of submicron or even angstrom size which is related to the submicron dimples on the fractographs.

The goal of this investigation is to understand how microstructural changes attending strength changes affect the fracture mechanism and fracture toughness in an 18 Ni, 300 grade maraging steel. In the 18 Ni, 300 grade maraging material, the fracture appearance changes as the strength is increased and the corresponding toughness decreases. The appearance change is evidently related to the microstructural features controlling the fracture process. The relative importance of the void initiation, growth, and coalescence stages of fracture is being examined as a function of strength.

In order to attain the goals of this program by clarification and correction of possible errors in the model proposed above, experimental evidence is necessary. In support of an understanding of the inverse relationship between strength and toughness the following work is necessary to complete this investigation.

1. TEM surface replicas will be used to further characterize the range in inclusion size, the inclusion shapes, and their orientation with respect to the martensite lath morphology.
2. Quantitative metallography will be used to assess, by type, the size and spatial distribution of the second-phase impurity inclusions present in the 300 grade maraging steel.
3. Thin foil TEM will be used to characterize the strengthening precipitates, related substructure, and deformation modes. In particular, TEM

selected area electron diffraction will be used to identify strengthening precipitates and determine if there are any compositional and/or structural changes in the precipitates as a function of the aging conditions.

4. In the overaged condition, there is a tendency for the body-centered cubic martensite to revert to the equilibrium face-centered cubic austenite. The degree of reversion will be examined by Mössbauer spectroscopy.

5. Plane-strain fracture toughness testing as characterized by valid K_{IC} measurements will be performed at progressively lower strength levels to add to the data in Table II. One-inch thick compact tension and 2.0-inch thick three-point bend K_{IC} specimens will be used for testing material in these lower strength levels.

6. The occurrence of intergranular fatigue in air at low ΔK levels will be corrected either by increasing ΔK where possible or by fatiguing in a protective argon atmosphere.

7. Quantitative fractography of the smooth tensile and K_{IC} fracture surfaces will be analyzed by replica TEM fractographic analysis. This work will be supplemented by SEM work as dictated by the experimental findings.

8. The fracture mechanism as a function of strength will be studied using metallographically sectioned tensile specimens of the 300 grade alloy which have been strained at 20°C (68°F) to various levels short of final failure. Optical as well as TEM replication techniques may be required to resolve submicron microstructural features indicated in the fractographic study above. The sectioned tensile technique will provide a key tool by which to directly relate the microstructural features such as inclusions and possibly strengthening precipitates which contribute to the various stages of fracture. It should further indicate the exact mechanism of void nucleation-particle cracking or interface decohesion as a function of strength.

CONCLUSIONS

One may summarize the findings of this investigation to date as follows:

1. Fatigue precracked Charpy and valid K_{IC} data clearly indicate that there is a significant inverse relationship between strength and toughness in the room temperature tested 18 Ni, 300 grade maraging steel.
2. Failure occurs at room temperature by the dimpled rupture process at all strengths considered.
3. This heat of 300 maraging steel contains cuboidal, $Ti(C,N)$ and elongated and irregular Ti_2S second-phase impurity inclusions.
4. The first voids are formed at the largest impurity inclusions with smaller inclusions becoming active void nucleation sites as plastic deformation proceeds.
5. With increasing strength, the dimples which cover the fracture surfaces decrease in size from as large as 10-20 μm to less than 1 μm in diameter.
6. The decrease in dimple size with increasing strength and/or overaging can be traced to the microstructure. Evidently, at the lowest strength levels considered, only the very largest inclusions from the entire population present in the material fail, forming voids which contribute to the fracture process. As the strength is increased, a larger fraction of the total size distribution of inclusions can act as void initiation sites. The result is a decrease in fracture toughness.
7. Environmental enhanced corrosion fatigue is responsible for the intergranular fatigue fracture in this material. Presumably oxygen and

water vapor are the combination causing the transition in fracture modes in fatigue. The branched intergranular crack tip is detrimental to valid plane-strain fracture toughness testing. The fracture mode can be returned to transgranular fatigue by cycling at sufficiently high ΔK or by operating in an oxygen-moisture free environment such as argon.

ACKNOWLEDGEMENTS

This work was performed under a research grant from the National Aeronautics and Space Administration. Two members of that organization, Messrs. W. D. Klopp and W. F. Brown, Jr., have been a source of continuing help and support. The comparison fatigue precracking of toughness specimens was performed by Dr. D. Young of the Westinghouse Research Laboratories. Conversations with R. J. Henry of Teledyne Vasco have been helpful during this investigation.

REFERENCES

1. J. A. Psioda and J. R. Low, Jr., "The Effect of Microstructure and Strength on the Fracture Toughness of an 18 Ni, 300 Grade Maraging Steel," NASA Technical Report No. 6, Department of Metallurgy and Materials Science, Carnegie-Mellon University, August 1974.
2. L. Roesch and G. Henry, Electron Microfractography, ASTM STP 453 (1969) p. 3.
3. G. J. Spaeder, R. M. Brown and W. J. Murphy, Trans. ASM, 60 (1967) p. 418.
4. T. B. Cox and J. R. Low, Jr., "An Investigation of the Plastic Fracture of High Strength Steel," NASA Technical Report No. 5., Department of Metallurgy and Materials Science, Carnegie-Mellon University, May 1973. (See also, Met. Trans., 5 (June 1974) p. 1457).
5. F. W. Jones and W. I. Pumphrey, JISI, 163 (1949) p. 121.
6. S. Floreen, "The Physical Metallurgy of Maraging Steels," in: Metalurgical Reviews, 126 (1968) p. 115.
7. W. A. Spitzig, J. M. Chilton and C. J. Barton, Trans. ASM, 61 (1968) p. 635.
8. M. J. Fleetwood, G. M. Higginson and G. P. Miller, British Journal of Applied Physics, 16 (1965) p. 645.
9. T. Boniszewski and E. Boniszewski, JISI, 204 (1966) p. 360.
10. C. F. Tipper, Metallurgia, 39 (1948) p. 133.
11. I. G. Palmer, G. C. Smith and R. D. Warda, Inst. Phys. and Phys. Soc. Conf. Series, No. 1 (1966) p. 53.
12. D. P. Clausing, Trans. ASM, 60 (1967) p. 504.
13. J. P. Tanaka, C. A. Pampillo and J. R. Low, Jr., ASTM STP 463 (1970) p. 191.
14. A. J. Birkle, R. P. Wei and G. E. Pellissier, Trans. ASM, 59 (1966) p. 981.
15. A. J. Birkle, D. S. Dabkowski, J. P. Paulina and L. F. Porter, Trans. ASM, 58 (1965) p. 285.
16. D. M. Fisher and A. J. Repko, Journal of Materials, JMLSA, 7, No. 2 (1972) p. 167.
17. M. H. Jones and W. F. Brown, Jr., Review of Developments in Plane Strain Fracture Toughness Testing, ASTM STP 463 (1970) p. 63.

18. J. E. Srawley, Second International Conf. on Fracture, Brighton, Sussex, England (1969) p. 131.
19. Damage Tolerant Design Handbook, A Compilation of Fracture and Crack-Growth Data for High-Strength Alloys, MCIC-HB-01, Metals and Ceramics Information Center, Battelle Columbus Laboratories, Air Force Materials Lab., December 1972.
20. A. Gangulee and J. Gurland, Trans. TMS-AIME, 239 (1967) p. 269.
21. J. N. Goodier, J. Appl. Mech., Trans. ASME, 55 (1933) p. 39.
22. R. H. Edwards, J. Appl. Mech., 18 (1951) p. 19.
23. J. Gurland and J. Piateau, Trans. ASM, 56 (1963) p. 443.
24. D. Broek, "A Study on Ductile Fracture," Ph.D. Thesis, Delft, Netherlands, 1971.
25. C. Zener, Fracturing of Metals, ASM, Metals Park, Ohio (1949) p. 3.
26. A. N. Stroh, Prcc. Roy. Soc., (London), A223 (1954) p. 404.
27. M. F. Ashby, AIME Met. Soc. Conf., 47 (1968) p. 143.
28. F. A. McClintock, "On the Mechanics of Fracture from Inclusions," in Ductility, ASM, Metals Park, Ohio (1968) p. 255.
29. A. S. Argon, J. Im and R. Safoglu, Met. Trans., 6A (1975) p. 825.
30. A. S. Argon and J. Im, Met. Trans., 6A (1975) p. 839.
31. J. Gurland, Acta Met., 20 (1972) p. 735.
32. R. H. Van Stone, R. H. Merchant and J. R. Low, Jr., ASTM STP 556 (1973) p. 93.
33. M. A. Greenfield and H. Margolin, Met. Trans., 3 (1972) p. 2649.
34. D. E. Passoja and D. C. Hill, "Quantitative Microfractography II - Particle Distribution Curves and Their Relationship to Fracture Toughness," Technical Report TTC-37, Tarrytown Technical Center, Union Carbide Corp., Tarrytown, New York, June 1973.
35. D. E. Passoja and D. C. Hill, Met. Trans., 5 (1974) p. 1851.
36. S. Floreen and H. W. Hayden, Scripta Met., 4 (1970) p. 87.
37. J. R. Rice and D. M. Tracey, Journal Mech. Phys. Solids, 17 (1969) p. 201.

38. G. T. Hahn and A. R. Rosenfield, "Metallurgical Factors Affecting Fracture Toughness of Aluminum Alloys," Presented at the 5th Annual Spring Meeting of the Met. Soc. AIME, June 1973; also, Met. Trans., 6A (1975) p. 653.
39. D. F. Stein and W. C. Johnson, Met. Trans., 5 (1974) p. 549.
40. W. F. Brown, Jr. and J. E. Srawley, Plane Strain Crack Toughness Testing of High Strength Metallic Materials, ASTM STP 410, ASTM (1967).
41. J. E. Srawley, M. H. Jones and W. F. Brown, Jr., Materials Research and Standards, MTRSA, 7, No. 6 (1967) p. 262.
42. S. Floreen and R. F. Decker, Trans. ASM, 55 (1962) p. 518.
43. "Standard Method of Test for Plane Strain Fracture Toughness of Metallic Materials," ASTM Designation E399-74, ASTM Standards, Part. 31.
44. T. J. Koppelaar, "Dynamic Fracture Toughness Measurements Using Pre-cracked Charpy Samples," Aeronutronic Division of Philco-Ford Corporation, Newport Beach, California (1973).
45. J. L. Shannon, Jr., NASA Lewis Research Center, Cleveland, Ohio, unpublished research.
46. P. W. Bridgman, Studies in Large Plastic Flow and Fracture, McGraw-Hill, New York (1952) p. 9.
47. R. H. Van Stone, Carnegie-Mellon University, private communication.
48. R. H. Van Stone, J. R. Low, Jr. and J. L. Shannon, Jr., "The Effect of Microstructure on the Fracture Toughness of Titanium Alloys," NASA Technical Report No. 2-Ti, Department of Metallurgy and Materials Science, Carnegie-Mellon University, December 1974.
49. Irwin Miller and John E. Freund, Probability and Statistics for Engineers, Prentice-Hall, Inc., Englewood Cliffs, N. J. (1965) p. 169.
50. L. F. Van Swam, R. M. Pelloux and N. J. Grant, Met. Trans., 6A (1975) p. 45.
51. H. J. Rack and D. Kalish, Met. Trans., 2 (1971) p. 3011.
52. D. Young and E. Wessel, Westinghouse Research Labs., Pittsburgh, Pa., private communications.

APPENDIX A
RESULTS OF INDIVIDUAL PLANE STRAIN
FRACTURE TOUGHNESS TESTS

The results of the individual plane strain fracture toughness (K_{Ic}) tests conducted during this study are listed in tabular form in this appendix. Data presented are valid per the requirements of ASTM E399-74 unless otherwise noted. The specimens aged at 399°C (750°F) for 3 hours have been the only invalid results to date.

APPENDIX A (continued)

RESULTS OF INDIVIDUAL PLANE STRAIN FRACTURE TOUGHNESS TESTS

Material: 18 Ni, 300 Grade Maraging Steel

Testing Conditions	Specimen Identification	Specimen Thickness B (in.)	Specimen Width w (in.)	Crack Length a (in.)	K_{Ic} (ksi $\sqrt{in.}$)	2.5 $(K_{Ic}/\sigma_y)^2$ (in.)
20°C(68°F) $\sigma_y = 299.6$ ksi Compact Tension Specimen LT Orientation Age: 427°C(800°F), 100 hrs.	KA28A-100	0.749	1.498	0.785	50.6	0.071
	KA9B-100	0.749	1.498	0.772	50.7	0.072
	KA1B-100	0.749	1.498	0.809	51.4	0.074
					50.9 Average	
20°C(68°F) $\sigma_y = 246.3$ ksi Compact Tension Specimen LT Orientation Age: 538°C(1000°F), 3 hrs.	KA16B1	0.749	1.495	0.815	64.6	0.172
	KA20A1	0.749	1.497	0.791	66.8	0.184
	KA25A1	0.749	1.494	0.795	69.2	0.192
	KA20B1	0.749	1.490	0.788	67.3	0.187
					66.7 Average	
20°C(68°F) $\sigma_y = 268.8$ ksi Compact Tension Specimen LT Orientation Age: 482°C(900°F), 3 hrs.	KA889	0.749	1.495	0.764	77.8	0.209
	KA4A9	0.749	1.492	0.765	78.5	0.213
	KA21A9	0.749	1.492	0.731	78.4	0.213
					78.2 Average	
20°C(68°F) $\sigma_y = 225.1$ ksi Compact Tension Specimen LT Orientation Age: 427°C(800°F), 3 hrs.	KA27B8	0.750	1.497	0.776	93.6	0.432
	KA23A8	0.749	1.495	0.759	95.7	0.452
	KA16A8	0.749	1.489	0.813	90.6	0.405
	KA10E8	0.749	1.500	0.818	106.6	0.561
					96.6 Average	

APPENDIX A (continued)

RESULTS OF INDIVIDUAL PLANE STRAIN FRACTURE TOUGHNESS TESTS

Material: 18 Ni, 300 Grade Maraging Steel

Testing Conditions	Specimen Identification	Specimen Thickness B (in.)	Specimen Width W (in.)	Crack Length a (in.)	K _{Ic} (ksi/in.)	$\frac{2.5 (K_{Ic}/\sigma_y)^2}{(in.)}$
20°C(68°F) $\sigma_y = 198.3$ ksi Compact Tension Specimen LT Orientation Age: 399°C(750°F), 3 hrs.	KA19A75	0.749	1.501	0.795	85.2 (a)	0.462
	KA17B75	0.749	1.498	0.795	99.5 (a)	0.629
	KA2-75	0.999	1.996	1.002	95.8 (a)	0.584
	KA3-75	0.999	1.999	0.997	136.5 (a,b,c)	1.185
	6-750	0.999	1.999	0.926	217.3 (a,b,c)	3.002
	5-750	0.999	1.998	1.005	149.5 (a,b,c)	1.421
					130.6 Average	

- (a) This is not a valid K_{Ic} value because the maximum load exceeds the 5% secant load by more than 10%.
- (b) This is not a valid K_{Ic} value because $B < 2.5 (K_{Ic}/\sigma_y)^2$.
- (c) This is not a valid K_{Ic} value because $a < 2.5 (K_{Ic}/\sigma_y)^2$.